21. LITHOLOGIC AND CHEMICAL STRATIGRAPHY AT DEEP SEA DRILLING PROJECT SITES 417 AND 418

M. F. J. Flower,[1] W. Ohnmacht,[2] P. T. Robinson,[3] G. Marriner,[4] and H.-U Schmincke[2]

ABSTRACT

Chemical compositions of basalts, detailed lithologic data, and stable magnetic inclinations are used to define an eruptive stratigraphy for the basement sections at Holes 417D and 418A. A maximum of 25 eruptive units, comprising three major sequences, are recognized in the 365-meter-thick section at Hole 417D, and a maximum of 54 eruptive units grouped into seven eruptive cycles are defined in the 544 meters penetrated at Hole 418A. The rocks in Hole 417A are too altered to permit detailed stratigraphic analysis.

The freshness of the rocks at Holes 417D and 418A suggests that the basement was sealed off shortly after formation by sedimentation and growth of secondary phases in the lava pile. Several horizons marked by the presence of breccia, by changes in magnetic inclinations and chemical compositions, and by increased alteration are believed to reflect major quiescent intervals in the eruptive record. These define a pattern of episodic eruption, with each episode possibly derived from a separate magma reservoir system. Variations in downhole magnetic inclinations suggest that crustal deformation occurs during each eruptive cycle, and that oscillatory lateral migration of the active zone may occur before a crustal section is complete.

Chemical variation of the basalts is not extensive and is dominated by fractionation of olivine, plagioclase, clinopyroxene, and spinel. Phenocryst movement during eruption and flow is fairly complex, but accumulation of plagioclase at or near the site of initial crystallization is a widespread phenomenon. Most magmas had reached a low-pressure cotectic stage by the time of eruption, but relict clinopyroxenes indicate an earlier stage of fractionation.

Dikes were intersected in the lower part of Hole 418A and correspond chemically to flows 130 meters higher in the section. These may represent the top of an underlying dike complex, originally forming near-surface feeder conduits, but now buried by subsequent eruptions.

INTRODUCTION

This paper presents chemical analyses of 205 whole-rock samples from Sites 417 and 418, drilled in Cretaceous basement in the western Atlantic Ocean on DSDP Legs 51, 52, and 53 (Figure 1).

We have integrated these data with shipboard observations of lithologic and magnetic stratigraphy and chemical variation of basaltic glass (Byerly and Sinton, this volume). Our main aim is to establish a chemical stratigraphy of the basement sections in Holes 417D and 418A in order to interpret igneous processes at the Cretaceous mid-ocean spreading axis. We proceed by defining eruptive units and major quiescent intervals, and then examine the relation between eruptive chronology and compositional variation of the basalts. From these relationships, the sampled section is interpreted in terms of dynamic crustal construction processes.

ANALYTICAL TECHNIQUES

Eight samples from Hole 417A, 45 from Hole 417D, and 152 from Hole 418A were analyzed for major elements at Bochum, West Germany, while a selection of 71 samples from Hole 418A were analyzed for Sr, Y, Zr, Rb, and Nb at Bedford College, London, England. Samples were carefully selected for analysis from representative portions of all flow units identified onboard ship so as to represent all major lithologic types. A few extremely altered specimens were analyzed, particularly from Hole 417A. These were not representative of original basalt compositions and served only to monitor alteration processes.

[1]Dept. of Mineral Sciences, Museum of Natural History, Smithsonian Institution, Washington, D.C. at time of cruise. Present address: 25 Willes Road, London NW5, England.

[2]Institut für Mineralogie der Ruhr-Universität, D-4630 Bochum, West Germany.

[3]Department of Geological Sciences, University of California, Riverside, California.

[4]Department of Geology, Bedford College, London NW1, England.

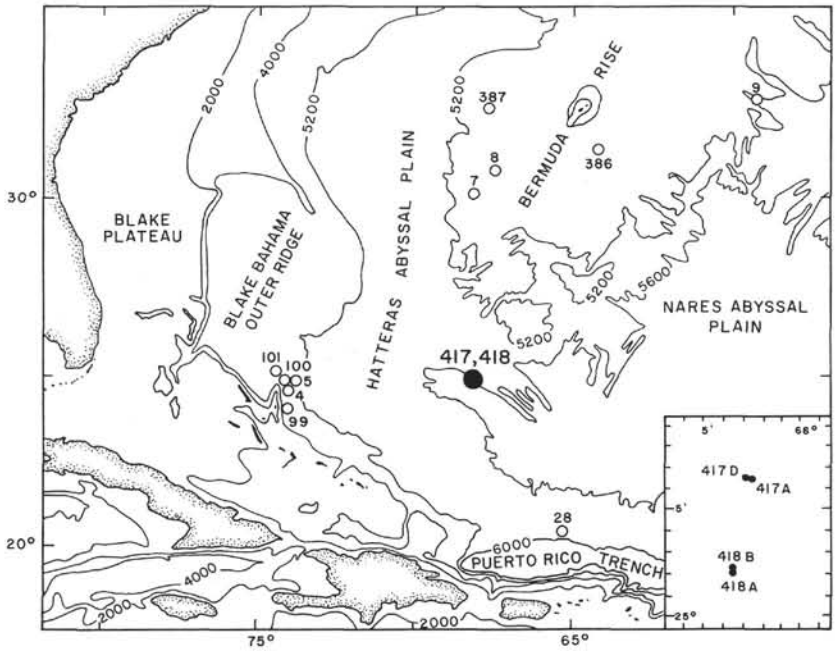

Figure 1. *Location map of Sites 417 and 418 at the southern end of Bermuda Rise, western Atlantic Ocean.*

Major oxides were determined by X-ray fluorescence, using a Philips PW 1410 under conditions as tabulated:

	SiO_2	Al_2O_3	P_2O_5	Fe_2O_3	K_2O	CaO	TiO_2
Tube	Cr						
Generator	50Kv, 30 mA				45 Kv, 18 mA		
Detector	flow counter (1.7 Kv)						
Path	vacuum (0.3 Torr)						
Collimator	coarse				fine		
Crystal	PE				LiF (200)		
Line	K						
Sample holder	electrolyte Cu						

Glass disks were prepared of: (a) international standards; (b) three Columbia River basalt samples (courtesy of T. L. Wright); (c) interlaboratroy comparison specimen, DSDP Sample 417A-44-3, 58-68 cm; and (d) DSDP Leg 51, 52, and 53 rock powders. The following proportions were used: 6.39 g $Na_2B_4O_7$ dried at 550°C (Spectromelt B10, Merck 6304) and 0.71 g rock powder dried at 1000°C. Unpolished disks were analyzed after confirmation that grinding and polishing made no difference in the analyses. The raw data were corrected for background and drift. Least-squares calibration curves were computed for each oxide, using the data of Abbey (1973) multiplied by loss-on-ignition (LOI) factors. LOI was determined on powders dried at 110°C for 24 hours. No corrections were made for Ca-P spectral interferences, however; the error for P is thought to be negligible because unknowns and standards are similar in composition.

Determinations of FeO, Na_2O, MnO, CO_2, and H_2O^+ were made potentiometrically, by atomic absorption, by coulometric titration (CTA-5 analyzer), and by coulometric Karl Fischer titration (Aquatest analyzer). Analytical results are given in Table 1. The interlaboratory comparison sample 15 is included in Table 1A as "Bochum Sample No. 250." Table 2 gives the DSDP designations for all specimens analyzed.

Trace elements were analyzed with a Philips PW 1212 XRF spectroscope on pressed powder pellets. Data for samples analyzed and standards are given in Table 1B.

LITHOLOGY

Basement recovery at Sites 417 and 418 averaged between 70 and 80 per cent and in some intervals exceeded 95 per cent. The high recovery, coupled with the freshness of most material cored from Holes 417D and 418A, makes possible an unexpectedly detailed study of the nature of oceanic Layer 2A. Drilled sequences at both Holes 417D and 418A appear to be typical of eruptive ocean crust, consisting of interlayered pillowed and massive basalt with lesser intercalations of breccia and sediment. Major differences from younger Atlantic basement (drilled on Legs 37, 45, 46, and 49) are the comparative scarcity of interlayered sediment and the greater abundance of breccia. Very low sedimentation rates at the time of crust formation (Orr and Miles, this volume) probably account for the lack of sediment, whereas the higher proportion of breccia probably reflects the higher degree of induration of the old crust. The high recovery enables us to identify all or most igneous cooling units, to correctly interpret their contacts and to identify highly altered layers. From these observations it is possible for the first time to make a realistic stratigraphic interpretation of the upper part of Layer 2.

As a first step in such an interpretation, we have subdivided the cored sequences into detailed lithologic subunits. A sub-unit is defined as a single igneous cooling unit, a breccia zone, or a sedimentary intercalation, regardless of any genetic association between contiguous sequences. In igneous sequences, cooling unit boundaries were identified from glassy selvages or from abrupt changes in grain size. In general, a unit boundary was inferred where a cooling

break traversed the core but not where it was vertical. Cooling units defined in this way include individual pillows with an average vertical thickness of about 0.5 meters (Robinson et al., this volume) and massive flows ranging from about 2 to 10 meters in thickness.

Breccia sequences and intercalated sediments are somewhat more difficult to interpret. Breccias may be "incipient" or comparatively well developed, and may vary in thickness from a few centimeters to about 1.5 meters. Some are hyaloclastites, clearly related to the process of pillow formation; others, termed "polymict" in this paper, are made up of angular clasts of variable lithology and composition, and probably represent accumulations of submarine talus. This type of breccia probably makes up lithologic Unit 6A in Hole 418A and Unit 9A in Hole 417D (Figures 2 and 3). Occasionally, a thick sequence of incipient breccia is bounded above and below by highly brecciated zones, possibly reflecting large fallen blocks buried by rubble and lava eruptions. However, distinctions between breccia types are difficult to make and for the purposes of unit definition we have assumed there to be only one lithologic type. Recognition of intercalated sediment is also difficult in many cases. Thick veins or patches of nonfossiliferous carbonate and smectite, with or without pyrite, often occur between cooling units, but it is not clear whether these are altered sediments or secondary mineral deposits. The euxinic bottom-water conditions during crust formation and the mixed (silica-carbonate) nature of these materials suggest that many are lithified sediment. Thus, we have interpreted such assemblages occurring between cooling units and exceeding 5 cm in thickness as sedimentary intercalations.

Using the criteria outlined above, we have recognized over 400 lithologic sub-units in Hole 417D and over 600 sub-units in Hole 418A. For each hole, units are numbered consecutively downhole and assigned an approximate sub-bottom depth computed from the core log. A listing of these units is available on request. For the purposes of this paper, however, we have used only the major lithologic units defined by the shipboard parties.

MAGNETIC STRATIGRAPHY

The magnetic stratigraphy at Holes 417D and 418A is complex, in common with most other basement sections drilled in the Atlantic Ocean. Stable inclinations are variable and often differ markedly from predicted dipole values. At Hole 418A, five downhole polarity reversals have been observed or inferred (Rigotti et al., this volume). Shipboard scientists of Legs 51, 52, and 53 do not agree on the interpretation of the magnetic data (Rigotti; Levi; Bleil and Smith; all, this volume), but it seems unlikely that secular changes of the magnetic field (Hall, in press; Watkins and Walker, 1977) can explain all of the downhole variation. We believe that the close coincidence of magnetic, lithologic, and chemical boundaries in the sequences at Sites 417 and 418 reflects deformation of discrete blocks during crustal construction. Thus, the magnetic pattern may provide a record of dynamic processes in the overall tectonic evolution of the active zone. However, interpretation of drill core data is complicated by the lack of sample control compared to subaerial lava flows, and the difficulty of testing tilting or rotation models. For this reason, we have attempted to identify magnetic "units" in the core, each unit reflecting a basalt sequence with closely similar stable inclinations. These units have been plotted against depth (Figures 2 and 3), together with shipboard lithologic divisions, in order to provide a framework in which to examine the downhole chemical variations. For a single cooling unit (pillow or massive unit) a single natural remanent magnetization (NRM) inclination is assumed to be representative of the whole unit. The validity of this assumption is supported by the uniformity of inclinations in relatively thick massive units with several magnetic data points. Some scatter of inclinations is observed in massive units near the base of Hole 418A, but those are believed due to the intrusion of dikes with polarities opposite to those of the intruded flows. Hyaloclastite and polymict breccias may be distinguished according to the range of inclinations measured for individual clasts: the former have inclinations similar to the enclosing lavas, while the latter have a nearly random distribution of inclinations.

BASALT PETROGRAPHY

Shipboard lithologic units for each site provide an accurate stratigraphic breakdown of the core. The updated lithologic subdivisions for Holes 417D and 418A are given in Figures 2 and 3. Before proceeding to a stratigraphic synthesis of rock chemistry and other properties, we shall give a brief summary of the basalt petrography. A more detailed description of basalt lithology is given in the Site Chapters in Part I of this volume.

Hole 417D

The 13 lithologic units identified in Hole 417D consist of pillowed basalt, massive basalt, and several thick horizons of basalt breccia. Plagioclase (An_{70-80}) is the main phenocryst phase in all basalts, but olivine and clinopyroxene are also present in small amounts. The plagioclase is relatively fresh and occurs as single-zoned grains and as glomerocrysts. Many crystals have abundant glass inclusions, often arranged in concentric bands. Clinopyroxene phenocrysts are present in most pillow basalts as fresh rounded crystals or glomerocrysts. Rounded clinopyroxene phenocrysts also occur at the base of the massive flow comprising lithologic Unit 1A. Phenocrystic olivine occurs in all lithologic units and is invariably altered to carbonate, with or without smectite. Dark red-brown spinel is present in lithologic Unit 4, either in the matrix or as microcrysts enclosed by clinopyroxene. The spinel crystals are rounded and have no oxidation rims. Subophitic plagioclase/clinopyroxene clots, with or without altered olivine, occur throughout the section, being distributed sporadically down to lithologic Unit 4 and widely below that level.

Groundmass textures in the pillow basalts range from quench to intersertal or intergranular. In massive units the groundmass has an "ophimottled" texture in which subophitic patches of plagioclase and clinopyroxene are partly surrounded by glass. Groundmass minerals in both pillowed and massive units are plagioclase, clinopyroxene, altered olivine, and minor iron oxides.

Vesicles or amygdules are abundant only in the uppermost parts of some massive flows (lithologic Units 2 and 3)

TABLE 1A
Major-Oxide Analyses of Whole-Rock Samples From DSDP Holes 417A, 417D, and 418A

Bochum Sample No.	Hole 417A								Hole 417D															
	110	120	160	180	210	220	240	250	1010	1020	1040	1060	1080	1110	1120	1140	1150	1170	1180	1185	1210	1240	1275	1280
SiO_2	46.90	47.12	48.53	47.05	47.03	48.55	49.06	49.25	46.99	48.28	47.72	48.67	47.30	48.05	48.91	49.62	47.76	47.54	48.17	48.10	47.81	49.36	48.41	47.93
TiO_2	1.28	1.27	1.32	1.32	1.29	1.45	1.39	1.42	1.54	1.43	1.32	1.28	1.32	1.32	1.36	1.34	1.28	1.35	1.35	1.41	1.28	1.49	1.38	1.35
Al_2O_3	18.05	16.89	16.92	16.63	16.14	16.93	16.47	16.33	17.54	17.06	16.39	16.78	16.84	17.44	17.39	17.21	17.46	16.90	16.44	18.42	16.15	17.92	16.69	16.88
Fe_2O_3	4.05	3.48	3.57	3.88	4.99	3.81	2.92	3.59	5.80	4.39	5.14	3.36	4.49	4.62	5.36	4.43	5.22	4.55	3.92	5.11	2.99	5.56	4.22	4.63
FeO	2.93	4.71	5.88	4.91	4.79	4.96	7.19	6.64	3.56	5.00	5.16	6.57	4.76	4.37	4.23	4.48	4.75	4.78	5.22	4.16	5.80	4.07	5.88	5.37
MnO	0.12	0.16	0.16	0.17	0.19	0.17	0.17	0.16	0.11	0.17	0.16	0.16	0.16	0.14	0.09	0.13	0.12	0.15	0.15	0.14	0.17	0.11	0.16	0.18
MgO	5.06	6.69	6.78	6.17	5.86	6.58	6.53	6.92	5.29	7.03	6.54	6.75	5.75	5.36	5.62	5.16	5.37	5.90	5.71	5.43	5.73	5.57	6.11	6.14
CaO	14.17	14.38	13.27	14.45	14.19	13.26	12.13	12.47	11.42	11.85	12.76	12.65	13.97	13.48	11.52	13.11	13.16	13.22	13.67	12.48	14.80	10.28	12.58	12.73
Na_2O	2.05	2.91	2.57	2.08	2.69	2.01	1.94	2.03	2.40	2.15	2.06	2.00	2.38	2.12	2.27	2.11	2.22	2.05	2.15	2.41	1.95	2.40	2.36	2.01
K_2O	0.95	0.09	0.03	0.18	0.33	0.03	0.07	0.08	0.55	0.07	0.27	0.05	0.06	0.29	0.38	0.05	0.15	0.20	0.08	0.35	0.06	0.79	0.36	0.26
P_2O_5	0.12	0.15	0.16	0.15	0.15	0.16	0.15	0.14	0.17	0.14	0.16	0.15	0.16	0.17	0.15	0.16	0.15	0.16	0.16	0.17	0.15	0.15	0.13	0.15
CO_2	2.16	1.48	0.38	1.38	1.46	0.43	0.13	0.13	1.93	0.84	1.18	0.18	1.78	1.15	0.46	0.61	0.83	1.50	1.61	0.75	1.98	0.34	0.67	0.95
H_2O^+	2.76	1.67	1.27	1.52	1.54	1.88	1.44	0.88	2.32	1.94	1.75	1.38	1.86	1.78	2.08	1.84	1.79	1.74	1.14	1.88	0.71	1.95	1.45	1.60
Sum	100.60	101.00	100.84	99.89	100.65	100.22	99.59	100.04	99.62	100.35	100.61	99.98	100.83	100.29	99.82	100.25	100.26	100.04	99.77	100.81	99.58	99.99	100.40	100.18
H_2O^-	1.23	1.34	0.75	1.21	0.94	1.04	0.53	0.11	1.92	2.22	0.99	1.14	1.51	1.70	2.20	1.23	1.54	1.67	0.54	1.97	0.45	1.81	0.94	0.85
FeO Total	6.57	7.84	9.09	8.40	9.28	8.39	9.82	9.87	8.78	8.95	9.78	9.59	8.80	8.53	9.05	8.47	9.45	8.87	8.75	8.76	8.49	9.07	9.68	9.54
Mg No.	60.90	63.32	60.14	59.77	56.09	61.35	57.37	58.65	54.94	61.38	57.49	58.74	56.93	55.98	55.67	55.22	53.49	57.36	56.91	55.64	57.72	55.40	56.09	56.57

Note: FeO Total = Total iron oxide expressed as FeO; Mg No. = Magnesium number = $Mg/(Mg + Fe^{+2})$, assuming $Fe^{+3} = 0.1 \times Fe^{+2}$.

TABLE 1A – *Continued*

Bochum Sample No.	Hole 417D – *Continued*																							
	1300	1320	1330	1400	1440	1460	1480	1500	1510	1520	1530	1540	1550	1560	1570	1590	1600	1620	1630	1650	1660	1670	1710	1720
SiO_2	47.10	46.83	48.53	48.96	47.19	47.91	48.11	48.07	48.99	46.94	48.34	48.81	47.90	46.59	47.82	47.64	48.73	47.70	49.47	46.39	47.31	47.13	48.46	47.98
TiO_2	1.27	1.30	1.26	1.13	1.42	1.49	1.52	1.61	1.55	1.39	1.46	1.40	1.52	1.63	1.60	1.55	1.54	1.53	1.48	1.56	1.34	1.37	1.34	1.36
Al_2O_3	16.66	15.88	17.89	18.20	16.16	15.78	15.94	16.84	17.07	16.05	17.09	15.18	15.81	15.41	15.57	15.56	15.29	15.70	15.74	15.72	17.70	16.42	16.78	16.72
Fe_2O_3	3.41	4.29	3.72	3.77	4.75	4.74	4.92	4.94	5.10	5.66	4.39	4.23	5.13	4.23	5.00	4.86	4.16	4.14	4.76	6.80	4.36	4.11	4.40	4.44
FeO	5.71	5.82	5.47	4.36	4.40	5.00	5.64	4.07	4.17	4.49	5.34	6.74	5.85	6.06	6.15	6.16	7.20	6.58	4.59	4.61	4.86	4.39	5.99	6.12
MnO	0.19	0.19	0.16	0.16	0.15	0.16	0.20	0.12	0.14	0.13	0.16	0.17	0.18	0.23	0.22	0.20	0.20	0.18	0.15	0.18	0.17	0.16	0.16	0.17
MgO	6.61	5.86	6.03	6.53	5.99	6.42	6.30	7.04	7.02	6.30	7.07	6.99	7.03	6.63	6.95	6.71	7.38	6.76	6.59	5.82	6.02	6.94	6.22	5.92
CaO	14.63	14.30	13.47	12.92	13.90	12.97	12.50	12.11	11.37	12.81	11.49	12.19	12.35	13.75	12.49	12.59	12.29	13.22	13.35	12.82	13.61	13.84	12.86	13.08
Na_2O	2.29	2.47	1.98	1.87	1.98	2.66	2.03	2.47	2.76	2.50	2.40	2.34	2.28	2.34	2.41	2.28	2.23	2.35	2.51	2.41	2.40	2.43	2.21	2.16
K_2O	0.07	0.27	0.05	0.04	0.34	0.32	0.21	0.13	0.24	0.38	0.22	0.09	0.11	0.14	0.05	0.08	0.04	0.04	0.08	0.46	0.08	0.05	0.04	0.04
P_2O_5	0.17	0.16	0.16	0.14	0.17	0.18	0.17	0.17	0.15	0.17	0.14	0.16	0.15	0.20	0.17	0.16	0.15	0.15	0.16	0.18	0.14	0.14	0.13	0.15
CO_2	1.85	1.78	0.87	0.39	1.98	1.34	0.96	1.22	0.67	1.51	1.24	0.42	0.55	1.55	0.46	0.38	0.27	0.76	0.35	1.58	1.25	1.70	0.40	0.52
H_2O^+	0.93	1.20	1.07	1.78	1.72	1.59	1.58	1.81	1.60	1.46	0.96	1.08	1.39	1.14	1.10	1.27	1.14	1.07	1.63	1.69	1.46	1.34	1.30	1.26
Sum	100.89	100.35	100.66	100.25	100.15	100.56	100.08	100.60	100.83	99.79	100.30	99.80	100.25	99.90	99.99	99.44	100.62	100.18	100.86	100.22	100.70	100.02	100.29	99.92
H_2O^-	0.88	0.71	0.87	1.38	0.93	1.25	1.16	1.61	1.52	0.94	0.75	0.74	1.37	1.16	1.33	1.06	0.91	1.13	1.57	1.11	1.36	1.27	1.01	1.06
FeO Total	8.78	9.68	8.82	7.75	8.67	9.27	10.07	8.52	8.76	9.58	9.29	10.55	10.47	9.87	10.65	10.53	10.94	10.31	8.87	10.73	8.78	8.09	9.95	10.12
Mg No.	60.37	55.05	58.05	63.02	58.28	58.37	55.87	62.59	61.85	57.08	60.63	57.28	57.61	57.62	56.90	56.31	57.71	57.03	60.04	52.33	58.10	63.45	55.85	54.21

TABLE 1A – *Continued*

Bochum Sample No.	Hole 417D – *Continued*					Hole 418A																		
	1730	1740	1760	1780	1790	10	15	20	30	40	50	60	70	80	90	100	103	106	110	120	130	136	140	150
SiO_2	48.56	48.87	48.41	49.72	48.52	46.74	48.98	48.41	48.29	47.76	47.12	49.10	48.77	49.40	49.19	48.37	50.18	49.44	48.47	48.91	49.48	49.27	49.45	49.12
TiO_2	1.36	1.41	1.32	1.39	1.25	1.09	1.22	1.22	1.20	1.17	1.10	1.15	1.10	1.10	1.15	1.11	1.09	1.07	1.03	1.03	1.06	1.05	1.09	1.12
Al_2O_3	16.56	17.01	16.78	16.05	16.93	17.18	18.27	17.50	17.88	17.70	16.89	17.03	16.09	16.30	16.69	16.11	16.63	16.30	16.65	16.68	16.41	16.78	16.78	16.33
Fe_2O_3	4.02	4.02	3.87	3.90	3.01	4.64	3.83	4.07	3.88	3.88	3.89	3.96	3.57	3.00	3.26	3.05	3.01	3.06	2.69	2.88	2.98	2.09	3.42	3.24
FeO	6.41	5.40	6.33	6.74	6.95	4.16	4.79	4.50	3.87	3.80	4.44	5.00	5.77	6.53	5.88	6.10	6.28	6.24	5.94	6.20	6.32	6.91	5.38	6.29
MnO	0.17	0.22	0.18	0.17	0.19	0.11	0.12	0.12	0.14	0.11	0.14	0.12	0.15	0.17	0.16	0.17	0.16	0.16	0.18	0.17	0.16	0.16	0.15	0.17
MgO	6.41	6.48	6.57	6.81	7.23	6.59	6.86	7.13	7.20	6.96	6.73	7.08	7.44	7.34	6.95	6.45	6.92	7.39	6.76	7.47	7.57	7.42	7.18	7.37
CaO	12.84	12.72	12.88	12.29	12.20	13.22	11.13	11.40	11.18	11.99	14.09	11.84	12.47	12.66	12.82	13.70	12.82	12.69	14.30	12.79	12.78	13.72	12.85	12.83
Na_2O	2.19	2.36	2.15	2.33	2.21	2.36	2.70	2.43	2.58	2.52	2.25	2.40	2.26	2.19	2.28	2.18	2.25	2.28	2.19	2.25	2.19	2.14	2.33	2.12
K_2O	0.06	0.05	0.04	0.10	0.08	0.12	0.18	0.08	0.45	0.18	0.13	0.10	0.08	0.06	0.07	0.10	0.07	0.08	0.09	0.09	0.09	0.09	0.06	0.05
P_2O_5	0.15	0.13	0.11	0.13	0.12	0.10	0.08	0.10	0.09	0.12	0.13	0.10	0.11	0.09	0.10	0.11	0.13	0.12	0.10	0.09	0.09	0.11	0.10	0.10
CO_2	0.43	0.22	0.12	0.11	0.31	1.88	0.51	0.14	0.0	1.01	1.60	0.12	0.12	0.11	0.14	0.84	0.18	0.24	1.34	0.23	0.18	0.17	0.25	0.08
H_2O^+	1.05	1.01	1.10	0.85	0.88	1.94	1.80	2.06	2.36	1.92	1.52	1.77	1.18	1.37	1.22	1.46	1.15	0.98	0.61	0.92	1.15	1.00	1.29	0.99
Sum	100.21	99.90	99.86	100.59	99.88	100.13	100.47	99.16	99.12	99.12	100.03	99.77	99.11	100.32	99.91	99.75	100.87	100.05	100.35	99.71	100.46	100.91	100.33	99.81
H_2O^-	0.83	0.94	0.79	0.49	0.64	2.61	1.37	2.45	2.56	2.54	1.57	1.70	0.83	0.66	0.96	1.24	0.53	0.43	0.53	0.76	0.82	0.43	0.84	0.84
FeO Total	10.03	9.02	9.81	10.25	9.66	8.34	8.24	8.16	7.36	7.29	7.94	8.56	8.98	9.23	8.81	8.84	8.99	8.99	8.36	8.79	9.00	8.79	8.46	9.21
Mg No.	56.40	59.25	57.53	57.34	60.23	61.53	62.76	63.86	66.43	65.89	63.17	62.59	62.63	61.67	61.47	59.60	60.90	62.44	62.06	63.22	62.98	63.07	63.20	61.83

TABLE 1A – *Continued*

Bochum Sample No.	Hole 418A – *Continued*																							
	152	154	156	158	160	170	180	190	193	197	220	225	230	245	248	250	260	266	270	280	286	290	300	303
SiO_2	48.02	48.51	48.72	48.67	48.89	47.81	49.34	49.02	49.00	48.28	47.36	47.88	47.04	48.73	47.36	47.01	47.65	47.29	47.84	47.41	47.34	47.79	47.19	46.82
TiO_2	1.08	1.15	1.14	1.06	1.24	1.14	1.13	1.32	1.27	1.14	1.14	1.14	1.10	1.06	1.05	1.23	0.98	1.12	1.13	1.15	1.22	1.09	1.16	1.16
Al_2O_3	16.97	17.18	18.11	17.36	15.99	16.68	16.80	17.51	16.96	18.84	18.18	17.48	16.06	18.37	18.11	19.43	18.44	17.64	18.03	17.94	16.90	17.56	18.50	17.38
Fe_2O_3	3.54	4.15	3.42	2.97	3.71	4.96	3.00	2.39	3.59	3.75	3.44	3.81	7.50	3.21	4.79	4.66	3.16	4.10	4.01	3.33	4.00	4.35	3.61	5.96
FeO	5.29	4.96	4.07	5.90	5.40	4.34	5.39	6.02	5.18	4.06	4.40	4.85	3.04	4.86	4.24	2.49	4.58	4.87	4.30	4.64	5.28	4.96	4.10	4.05
MnO	0.14	0.14	0.11	0.15	0.15	0.13	0.15	0.14	0.20	0.19	0.21	0.36	0.09	0.15	0.17	0.18	0.15	0.15	0.18	0.17	0.19	0.17	0.21	0.16
MgO	6.31	6.93	6.84	6.78	7.43	6.63	7.40	6.70	7.71	6.52	6.37	6.83	7.82	6.75	6.27	6.35	6.38	6.15	6.62	6.64	7.25	6.87	6.48	5.58
CaO	13.78	12.59	12.41	13.21	12.90	13.13	12.89	11.38	12.00	12.50	13.51	13.06	6.95	13.20	12.78	11.15	12.31	12.81	13.10	13.35	13.15	13.12	13.08	12.86
Na_2O	2.24	2.37	2.47	2.27	2.41	2.35	2.38	2.68	2.43	2.46	2.38	2.23	2.38	2.20	2.18	2.55	2.40	2.16	2.26	2.28	2.24	2.16	2.30	2.31
K_2O	0.08	0.09	0.07	0.09	0.05	0.19	0.08	0.34	0.06	0.21	0.18	0.28	2.28	0.05	0.41	0.66	0.71	0.80	0.23	0.14	0.12	0.13	0.10	0.59
P_2O_5	0.13	0.12	0.11	0.14	0.11	0.11	0.11	0.10	0.12	0.13	0.10	0.13	0.09	0.13	0.14	0.10	0.10	0.14	0.11	0.09	0.17	0.10	0.10	0.14
CO_2	1.01	0.45	0.80	0.61	0.42	0.98	0.17	0.50	0.33	0.91	1.67	0.89	1.22	0.45	0.84	1.16	1.14	1.30	0.80	1.82	0.78	0.76	0.78	1.06
H_2O^+	1.64	1.32	1.52	1.36	1.50	1.82	1.48	2.26	1.78	1.60	1.74	1.34	4.96	1.28	1.59	3.20	2.31	1.81	1.74	1.63	1.12	1.56	2.27	2.08
Sum	100.23	99.96	99.79	100.57	100.20	100.27	100.32	100.36	100.63	100.59	100.68	100.28	100.53	100.44	99.93	100.17	100.31	100.34	100.35	100.59	99.76	100.62	99.88	100.15
H_2O^-	1.12	1.39	1.56	1.03	1.42	1.76	1.04	2.66	1.50	1.88	2.07	1.49	4.74	1.23	1.52	3.07	2.33	1.36	2.16	2.24	1.22	1.89	2.21	1.63
FeO Total	8.48	8.69	7.15	8.57	8.74	8.80	8.09	8.17	8.41	7.43	7.50	8.28	9.79	7.75	8.55	6.68	7.42	8.56	7.91	7.64	8.88	8.87	7.35	9.41
Mg No.	60.10	61.73	65.94	61.54	63.24	60.38	64.92	62.39	64.97	63.96	63.23	62.54	61.78	63.80	59.74	65.78	63.49	59.25	62.88	63.76	62.29	61.03	64.08	54.53

TABLE 1A – *Continued*

Bochum Sample No.	Hole 418A – *Continued*																							
	310	320	330	340	342	346	348	350	360	370	375	380	395	400	420	425	430	435	440	450	460	462	464	470
SiO_2	48.23	47.95	46.70	47.94	48.44	48.38	47.06	46.74	47.20	47.90	47.15	47.38	47.03	48.31	47.26	47.20	47.26	48.24	47.43	48.35	47.02	48.12	47.23	46.89
TiO_2	1.24	1.27	1.14	1.17	1.20	1.16	1.17	1.20	1.08	1.11	0.95	0.92	0.96	0.96	0.97	0.95	0.89	0.92	0.97	0.95	1.03	1.00	1.05	0.98
Al_2O_3	18.08	18.79	17.07	16.93	17.86	17.25	17.85	17.64	18.30	17.48	17.66	17.24	18.01	18.26	18.03	17.59	17.84	18.43	18.54	18.77	18.34	17.60	17.75	17.17
Fe_2O_3	3.87	4.04	5.87	6.68	4.01	3.64	3.77	4.04	3.35	3.26	3.44	2.77	3.37	3.65	3.97	3.80	2.79	3.69	4.05	3.34	3.92	4.03	3.60	4.20
FeO	4.44	3.68	4.15	3.69	4.51	5.11	5.01	4.48	5.08	4.77	4.67	5.28	4.90	4.47	4.46	5.20	4.85	4.95	4.56	4.40	4.03	5.24	5.12	4.78
MnO	0.21	0.16	0.14	0.11	0.16	0.19	0.19	0.15	0.15	0.17	0.19	0.17	0.17	0.13	0.13	0.15	0.14	0.14	0.15	0.12	0.15	0.15	0.16	0.17
MgO	6.49	6.77	6.47	6.22	6.79	6.82	6.32	5.73	5.61	5.92	5.55	7.34	5.50	5.79	5.52	6.49	6.21	6.16	5.67	5.80	5.80	5.86	5.72	6.23
CaO	13.15	11.35	11.74	10.64	12.60	13.24	12.85	13.90	14.20	12.31	14.11	14.41	15.27	14.32	14.78	14.11	15.01	13.65	14.28	13.65	14.29	13.71	14.15	14.39
Na_2O	2.36	2.39	2.32	2.19	2.31	2.22	2.55	2.20	2.20	2.67	2.48	2.13	2.25	2.27	2.25	2.10	2.19	2.06	2.23	2.29	2.28	2.10	2.27	2.08
K_2O	0.08	0.48	0.48	1.25	0.26	0.16	0.47	0.61	0.31	1.18	0.37	0.08	0.10	0.15	0.05	0.05	0.16	0.03	0.03	0.11	0.22	0.04	0.10	0.06
P_2O_5	0.10	0.09	0.10	0.12	0.12	0.13	0.13	0.11	0.11	0.10	0.14	0.09	0.13	0.09	0.10	0.12	0.08	0.07	0.09	0.08	0.10	0.13	0.13	0.09
CO_2	0.53	0.34	0.73	0.35	0.68	0.78	0.67	1.71	1.06	1.10	1.29	1.77	1.69	0.77	1.15	0.98	1.99	0.32	0.64	0.40	1.62	0.56	0.88	1.45
H_2O^+	2.18	2.93	3.09	2.72	1.57	1.32	2.23	2.12	2.03	2.01	1.95	0.93	1.23	1.66	1.86	1.11	1.25	1.36	1.90	1.77	1.74	1.85	1.44	1.81
Sum	100.96	100.24	100.00	100.01	100.51	100.40	100.27	100.63	100.68	99.98	99.95	100.51.	100.61	100.83	100.53	99.85	100.66	100.02	100.54	100.03	100.54	100.39	99.60	100.30
H_2O^-	2.10	2.92	2.44	1.89	1.58	1.35	1.41	2.28	2.08	1.99	1.39	0.59	1.38	1.55	1.82	1.14	1.47	0.63	2.30	2.10	2.55	1.25	1.49	1.79
FeO Total	7.92	7.32	9.43	9.70	8.12	8.39	8.40	8.12	8.09	7.70	7.77	7.77	7.93	7.75	8.03	8.62	7.36	8.27	8.20	7.41	7.56	8.87	8.36	8.56
Mg No.	62.37	65.19	58.12	56.47	62.86	62.20	60.35	58.82	58.37	60.86	59.12	65.64	58.38	60.17	58.17	60.37	63.06	60.11	58.30	61.31	60.83	57.21	58.06	59.56

TABLE 1A – *Continued*

Bochum Sample No.	Hole 418A – *Continued*																							
	490	500	510	520	530	540	550	570	575	580	590	595	600	610	620	630	640	650	660	670	680	690	700	720
SiO_2	47.98	47.52	48.02	47.51	48.80	47.73	47.31	48.59	48.36	47.07	49.01	48.49	47.06	48.28	47.93	47.89	48.14	47.28	47.52	47.72	47.95	48.25	48.04	48.39
TiO_2	1.06	1.03	1.05	1.02	1.08	1.03	1.01	1.04	1.06	1.01	1.14	1.01	1.04	1.15	1.05	1.04	1.01	1.12	1.05	1.06	1.05	1.03	1.07	1.08
Al_2O_3	17.47	17.58	17.72	17.06	17.96	17.35	17.12	18.43	17.71	16.62	17.58	17.05	16.60	17.16	17.81	17.14	16.84	17.02	17.66	17.63	18.16	18.11	18.29	17.78
Fe_2O_3	4.73	4.00	4.61	3.46	3.97	3.76	3.73	3.79	4.87	3.86	3.86	3.39	4.10	4.25	4.52	3.96	3.20	4.69	4.70	4.24	4.77	3.90	4.66	4.07
FeO	4.66	5.37	4.69	5.86	4.72	5.59	5.18	4.72	4.68	5.28	4.98	5.92	5.26	4.98	4.72	5.49	5.91	4.93	4.46	5.11	4.55	5.32	4.42	5.31
MnO	0.16	0.16	0.14	0.16	0.13	0.15	0.16	0.13	0.14	0.16	0.13	0.15	0.17	0.15	0.16	0.16	0.16	0.18	0.15	0.17	0.12	0.15	0.14	0.17
MgO	6.00	5.91	5.39	6.67	5.85	6.18	6.56	6.08	5.07	6.49	6.36	7.35	6.15	5.68	5.60	6.18	7.40	5.84	5.47	5.60	4.98	5.92	5.22	6.23
CaO	13.41	13.67	13.87	13.55	13.37	13.69	14.04	13.24	13.83	13.87	12.87	12.79	14.47	13.71	13.86	13.49	12.95	14.05	13.99	14.01	13.75	13.49	13.70	13.19
Na_2O	2.20	2.13	2.19	2.09	2.23	2.12	2.03	2.18	2.20	2.01	2.25	2.09	2.09	2.26	2.14	2.15	2.26	2.16	2.10	2.05	2.12	2.10	2.21	2.18
K_2O	0.18	0.04	0.11	0.05	0.06	0.04	0.04	0.08	0.04	0.04	0.12	0.04	0.07	0.06	0.03	0.03	0.03	0.04	0.07	0.03	0.14	0.03	0.08	0.03
P_2O_5	0.09	0.09	0.09	0.10	0.09	0.10	0.10	0.08	0.12	0.10	0.09	0.12	0.10	0.10	0.09	0.10	0.07	0.10	0.08	0.09	0.09	0.08	0.09	0.08
CO_2	0.51	0.57	0.63	0.64	0.29	0.67	1.12	0.26	0.61	1.28	0.23	0.11	1.59	0.51	0.62	0.62	0.54	0.99	0.82	0.85	0.44	0.27	0.46	0.17
H_2O^+	1.86	2.08	2.15	1.78	1.71	1.97	1.62	1.93	1.52	2.31	2.27	1.45	1.80	2.07	2.23	2.20	1.87	2.17	2.24	1.85	2.32	1.71	2.15	1.91
Sum	100.31	100.15	100.66	99.95	100.26	100.38	100.02	100.55	100.21	100.10	100.89	99.96	100.50	100.36	100.76	100.45	100.38	100.57	100.31	100.41	100.44	100.36	100.53	100.59
H_2O^-	1.93	1.51	1.75	1.28	2.52	1.25	1.49	2.41	1.86	1.72	1.96	0.75	1.54	2.25	1.86	1.62	1.36	2.25	1.76	2.01	2.34	1.39	2.49	1.73
FeO Total	8.92	8.97	8.84	8.97	8.29	8.97	8.54	8.13	9.06	8.75	8.45	8.97	8.95	8.80	8.79	9.05	8.79	9.15	8.69	8.93	8.84	8.83	8.61	8.97
Mg No.	57.65	57.14	55.23	60.06	58.80	58.22	60.86	60.21	53.09	60.00.	60.35	62.37	58.17	56.62	56.32	58.00	63.01	56.36	56.02	55.94	53.26	57.57	55.08	58.42

TABLE 1A – *Continued*

Bochum Sample No.	Hole 418A – *Continued*																							
	730	740	750	760	770	780	790	800	810	820	830	840	850	860	870	880	890	900	910	920	940	950	960	970
SiO_2	48.38	48.38	49.14	48.14	47.49	48.29	48.08	48.48	47.86	47.14	48.66	48.19	47.75	47.38	47.70	49.04	47.73	47.66	47.73	47.53	48.14	47.79	47.88	48.16
TiO_2	1.13	0.95	1.31	1.28	1.24	1.20	1.21	1.42	1.58	1.49	1.54	1.57	1.34	1.35	1.27	1.31	1.25	1.31	1.29	1.31	1.22	1.24	1.32	1.27
Al_2O_3	16.77	18.33	15.60	15.18	16.81	16.44	16.39	17.01	16.51	15.94	15.37	15.58	17.46	17.34	16.48	16.79	16.70	17.47	16.98	16.21	16.31	15.92	16.08	15.71
Fe_2O_3	3.62	3.78	3.27	3.25	3.18	3.83	3.25	3.78	4.95	4.92	4.41	4.76	3.37	4.25	4.01	4.19	5.01	4.15	4.03	3.76	3.36	3.71	3.30	2.68
FeO	5.44	5.06	6.62	6.62	5.62	5.75	5.93	6.14	5.51	5.27	6.55	6.44	5.78	5.22	5.33	5.24	4.74	4.14	5.02	5.71	6.29	5.91	5.83	7.09
MnO	0.15	0.15	0.19	0.19	0.17	0.16	0.18	0.17	0.18	0.16	0.18	0.18	0.16	0.16	0.16	0.13	0.15	0.14	0.15	0.19	0.18	0.17	0.16	0.18
MgO	6.49	6.33	7.48	7.52	6.85	6.67	7.00	6.28	6.53	6.95	6.38	6.56	6.04	5.76	6.05	6.24	5.70	6.56	6.50	6.94	7.03	6.70	6.71	7.06
CaO	13.07	13.42	12.49	13.41	14.02	13.60	13.62	12.88	12.35	12.67	11.91	11.83	13.50	13.20	14.10	12.31	13.75	13.04	13.15	13.34	13.64	13.91	13.60	13.70
Na_2O	2.41	2.10	2.31	2.24	2.31	2.18	2.20	2.30	2.36	2.22	2.33	2.45	2.43	2.35	2.33	2.55	2.36	2.49	2.52	2.28	2.24	2.20	2.28	2.22
K_2O	0.25	0.02	0.05	0.06	0.05	0.03	0.04	0.09	0.04	0.04	0.08	0.30	0.13	0.26	0.09	0.31	0.34	0.04	0.04	0.05	0.04	0.05	0.09	0.06
P_2O_5	0.09	0.09	0.11	0.13	0.14	0.13	0.12	0.13	0.16	0.14	0.14	0.14	0.13	0.13	0.13	0.12	0.13	0.13	0.14	0.13	0.13	0.14	0.15	0.13
CO_2	1.43	0.17	0.32	1.06	1.25	0.81	0.89	0.37	0.38	1.13	0.19	0.40	1.15	1.08	0.98	0.18	1.00	1.14	0.76	0.95	0.92	1.34	1.44	1.12
H_2O^+	1.44	1.52	1.19	0.80	1.21	1.52	0.89	1.32	1.90	1.78	1.37	1.16	1.03	1.31	1.24	1.87	1.60	2.20	1.81	1.49	1.09	1.29	1.35	0.87
Sum	100.67	100.30	100.08	99.88	100.34	100.61	99.80	100.37	100.31	99.85	99.11	99.56	100.27	99.79	99.87	100.28	100.46	100.47	100.12	99.89	100.59	100.37	100.19	100.25
H_2O^-	2.29	1.67	1.26	0.89	1.00	1.25	0.98	1.32	1.90	2.17	0.77	1.22	1.21	1.38	1.44	1.92	1.52	2.52	2.26	1.68	1.10	0.77	1.36	0.62
FeO Total	8.70	8.46	9.56	9.54	8.48	9.20	8.85	9.54	9.96	9.70	10.52	10.72	8.81	9.04	8.94	9.01	9.25	7.87	8.65	9.09	9.31	9.25	8.80	9.50
Mg No.	60.16	60.22	61.28	61.45	62.04	59.47	61.53	57.11	57.01	59.18	55.10	55.31	58.10	56.30	57.80	58.35	55.50	62.76	60.33	60.69	60.43	59.44	60.67	60.05

TABLE 1A – *Continued*

Bochum Sample No.	Hole 418A – *Continued*																							
	980	990	1010	1040	1060	1070	1080	1090	1100	1110	1130	1140	1160	1170	1180	1190	1200	1210	1220	1230	1240	1250	1260	1270
SiO_2	47.90	48.26	49.11	48.96	47.48	47.02	49.05	48.33	47.61	48.31	49.36	48.52	49.17	48.62	48.95	49.78	48.69	49.59	49.22	48.56	49.28	48.75	49.52	49.41
TiO_2	1.20	1.21	1.31	1.28	1.27	1.24	1.39	1.22	1.22	1.22	1.24	1.20	1.29	1.29	1.24	1.22	1.43	1.19	1.31	1.19	1.14	1.13	1.33	1.38
Al_2O_3	16.21	16.37	15.32	15.88	15.97	16.02	16.48	16.53	15.84	15.90	16.17	15.51	15.29	15.74	16.22	17.40	14.81	17.32	16.27	16.68	17.37	17.28	16.27	15.20
Fe_2O_3	3.74	5.88	2.63	3.54	3.73	2.99	4.02	2.80	3.22	3.02	3.37	3.29	4.09	3.35	3.39	3.41	4.22	3.70	3.54	3.50	3.56	3.14	3.29	3.33
FeO	5.92	3.90	7.23	6.60	6.06	6.07	5.64	6.65	6.32	6.44	6.47	6.00	5.90	6.50	6.11	5.27	6.67	5.71	6.45	6.33	5.70	6.11	6.68	7.19
MnO	0.18	0.18	0.17	0.19	0.20	0.18	0.13	0.17	0.21	0.17	0.16	0.17	0.19	0.16	0.16	0.15	0.18	0.16	0.18	0.18	0.16	0.17	0.18	0.18
MgO	6.77	7.00	6.94	7.30	6.85	6.53	7.08	6.70	6.86	7.08	6.89	7.01	7.33	6.64	6.68	6.51	7.69	6.60	6.46	7.05	6.58	6.90	6.68	7.21
CaO	13.65	13.54	12.86	12.76	13.84	14.72	11.51	13.44	14.32	13.50	12.69	13.72	12.73	13.44	13.41	13.05	12.49	12.88	12.73	12.83	13.10	12.93	12.75	12.23
Na_2O	2.24	2.17	2.17	2.15	2.24	2.19	2.27	2.19	2.13	2.16	2.24	2.18	2.33	2.16	2.18	2.33	2.28	2.22	2.29	2.22	2.20	2.23	2.26	2.27
K_2O	0.04	0.04	0.07	0.04	0.05	0.05	0.47	0.07	0.05	0.09	0.05	0.11	0.07	0.07	0.06	0.05	0.04	0.06	0.07	0.03	0.03	0.03	0.05	0.07
P_2O_5	0.12	0.14	0.12	0.14	0.14	0.14	0.12	0.14	0.14	0.13	0.11	0.13	0.13	0.14	0.14	0.13	0.15	0.12	0.14	0.11	0.12	0.13	0.13	0.13
CO_2	0.84	0.87	0.71	0.31	1.15	1.90	0.26	0.90	1.61	1.23	0.36	1.41	0.57	1.08	0.94	0.49	0.31	0.17	0.37	0.14	0.26	0.13	0.45	0.22
H_2O^+	1.02	1.08	0.74	0.28	0.34	0.29	1.77	0.27	0.22	0.33	0.96	0.91	1.20	0.92	0.28	0.31	0.43	0.30	0.32	1.16	0.49	1.13	0.23	0.85
Sum	99.83	100.64	99.38	99.43	99.32	99.34	100.19	99.41	99.75	99.58	100.07	100.16	100.29	100.11	99.76	100.10	99.39	100.02	99.35	99.98	99.99	100.06	99.82	99.67
H_2O^-	1.01	1.15	0.93	1.20	1.35	1.25	2.96	0.89	0.81	1.04	0.77	0.85	1.29	0.64	0.67	1.06	1.64	0.92	0.84	1.09	1.04	0.98	0.66	0.70
FeO Total	9.29	9.19	9.60	9.79	9.42	8.76	9.26	9.17	9.22	9.16	9.50	8.96	9.58	9.51	9.16	8.34	10.47	9.04	9.64	9.48	8.90	8.94	9.64	10.19
Mg No.	59.60	60.64	59.40	60.15	59.54	60.13	60.74	59.65	60.09	61.00	59.46	61.28	60.75	58.54	59.60	61.23	59.78	59.63	57.56	60.08	59.92	60.97	58.37	58.88

TABLE 1A – *Continued*

Bochum Sample No.	1280	1290	1300	1310	Hole 418A – *Continued* 1320	1330	1340	1350	1360	1370	1380	1400	1410
SiO_2	49.03	48.87	48.96	48.96	48.57	47.80	48.91	47.70	48.30	47.66	48.60	48.75	48.63
TiO_2	1.18	1.13	1.10	1.13	1.19	1.31	1.26	1.12	1.23	1.12	1.20	1.13	1.16
Al_2O_3	16.93	16.25	15.14	15.34	15.55	14.99	15.32	17.48	17.59	17.14	17.78	17.18	17.19
Fe_2O_3	3.33	3.11	2.74	2.85	3.32	2.88	3.95	3.53	4.25	3.09	3.99	3.35	3.26
FeO	6.28	6.31	7.23	7.03	6.04	6.17	5.89	5.40	4.51	5.72	4.86	6.09	5.83
MnO	0.17	0.17	0.18	0.18	0.18	0.18	0.20	0.22	0.16	0.21	0.15	0.18	0.17
MgO	7.24	7.93	9.78	9.04	7.68	7.93	7.70	6.63	6.38	6.75	5.95	7.07	6.33
CaO	12.53	12.41	12.02	11.72	13.17	14.24	12.60	14.14	13.01	14.10	13.73	13.12	13.80
Na_2O	2.21	2.22	2.05	2.05	2.23	2.11	2.21	2.10	2.34	2.09	2.17	2.07	2.24
K_2O	0.05	0.04	0.08	0.10	0.05	0.08	0.09	0.04	0.17	0.05	0.07	0.04	0.06
P_2O_5	0.12	0.12	0.12	0.11	0.15	0.14	0.13	0.15	0.11	0.12	0.14	0.13	0.12
CO_2	0.12	0.17	0.17	0.12	0.93	1.89	0.49	0.97	0.80	1.08	0.57	0.29	0.77
H_2O^+	0.50	1.20	0.55	1.49	0.44	0.60	1.25	0.46	0.81	0.33	0.76	0.58	0.40
Sum	99.69	99.93	100.12	100.12	99.50	100.32	100.00	99.94	99.66	99.46	99.97	99.98	99.96
H_2O^-	0.70	0.95	0.55	0.62	1.01	1.04	1.33	1.68	2.65	1.42	2.33	1.22	1.21
FeO Total	9.28	9.11	9.70	9.59	9.03	8.76	9.44	8.58	8.33	8.50	8.45	9.10	8.76
Mg No.	61.23	63.79	67.11	65.59	63.25	64.68	62.26	61.00	60.77	61.64	58.76	61.11	59.37

TABLE 1B
Trace-Element Analyses of Whole-Rock Samples From DSDP Hole 418A

Bedford College XRF Numbers	Nb	Y	Sr (ppm)	Rb	Zr	Bochum Code No.
865901	4	24	120	0	56	40
867801	4	25	105	1	56	60
864701	5	23	115	0	54	90
866801	5	21	101	0	55	120
863701	4	21	108	2	49	130
866701	4	24	106	2	43	140
866481	5	23	106	0	64	150
868101	7	23	104	1	62	290
864901	4	25	116	0	52	300
864201	5	25	112	2	61	310
865701	4	25	152	0	45	360
865001	5	21	106	5	45	460
863101	4	25	121	2	48	470
864601	5	24	100	0	49	480
864101	5	23	101	0	44	500
865301	5	27	100	1	62	510
866901	5	22	98	0	48	520
866601	4	21	99	2	43	540
864001	4	23	106	0	50	550
864301	2	21	105	1	42	580
864501	4	25	110	0	49	600
866501	4	24	94	0	53	610
868001	2	24	105	0	52	620
865201	5	23	101	1	51	660
867901	5	25	114	0	51	670
863501	4	22	95	0	44	680
865501	4	23	100	0	48	740
861501	4	27	115	0	63	770
861901	5	26	112	0	62	790
862401	4	29	100	0	77	800
867601	6	31	114	1	85	810
870701	6	30	112	0	78	820
863901	7	32	104	0	74	830
865801	5	28	108	1	69	860
863001	6	28	108	1	66	870
861801	4	26	99	9	60	890
866201	5	25	106	0	61	910
865101	5	29	108	0	66	920
861601	2	28	103	0	59	940
866101	5	23	114	0	65	950
867501	5	26	113	1	63	960
862501	4	26	108	0	71	980
862801	2	26	109	1	62	990
862301	7	27	132	3	65	1010
867101	4	25	100	0	67	1040
867701	6	27	103	0	66	1060
8664A1	5	26	114	0	67	1070
863801	2	26	110	1	59	1100
862201	7	27	105	1	74	1110
862601	4	24	108	4	68	1130
867301	2	25	111	2	61	1140
866001	2	26	111	2	66	1150
863401	7	28	108	1	66	1160
868201	4	28	108	0	67	1170
865401	6	28	106	0	63	1180
870801	2	26	99	0	52	1210
862101	6	28	100	1	65	1220
863601	5	24	98	2	49	1250
863301	5	28	98	0	70	1260
866301	4	30	97	0	69	1270
862701	5	26	97	0	59	1280
865601	4	26	98	0	58	1290
861701	6	27	87	0	58	1300
867401	5	25	87	2	63	1310
864801	4	28	103	0	57	1320
867001	5	22	130	4	59	1330
864401	5	28	103	0	63	1340
863201	5	23	102	0	70	1350
862001	7	22	103	0	53	1370
862901	5	27	97	0	54	1400
867201	4	26	102	0	60	1410
Standards						
108801	96	26	1288	46	248	BR
110601	14	33	313	44	174	BCR
110301	14	21	673	70	228	AGV
256601	228	94	6	2014	758	MICA-FE
110401	3	0	3	2	2	PCC-1
868401	61	22	727	76	254	B-BO
868301	6	39	126	0	127	AII
870601	16	25	72	361	187	G-BO

and in the pillow basalts of Unit 4. They are usually filled with carbonate accompanied by brown or green smectite.

Hole 418A

The basement section at Site 418 is similar to that at Site 417. Sixteen lithologic units were identified in Hole 418A, comprising pillowed and massive flows, various breccias, and a series of dikes (lithologic Unit 15) at the base of the section. Most basalts are moderately to sparsely phyric, aphyric varieties occurring only rarely in Units 14A through C. Phenocrysts are mostly of plagioclase with lesser amounts of clinopyroxene, olivine, spinel, and possibly some iron-titanium oxides. Plagioclase occurs as euhedral to rounded crystals and forms up to 20 modal per cent. Compositions range from An_{80} to An_{60} with both normal and oscillatory zoning. Glass inclusions are common and occur irregularly distributed or in zonal arrangement. Bubbles within these inclusions suggest the presence of a fluid phase at the time of crystallization. Except for lithologic Unit 9, all the basalts contain 3 to 5 modal per cent of olivine phenocrysts, most of which is replaced by brown smectite and/or carbonate. Olivine pseudomorphs are euhedral to rounded. In lithologic Units 6 and 8 rounded crystals of fresh olivine coexist with pseudomorphs, suggesting two generations of olivine crystallization. Small amounts of phenocrystic clinopyroxene occur in lithologic Units 6 through 15. These crystals are fresh, subhedral to anhedral or rounded, and typically form glomerocrysts with olivine and plagioclase. Euhedral spinel is a common phase in lithologic Unit 6. It is dark red-brown and often rimmed by magnetite. The spinel occurs both as single grains and as inclusions in plagioclase and olivine.

Groundmass textures vary from fine-grained quenching pillow basalts to medium-grained subophitic or "ophimottled" in massive flows. Skeletal crystals of plagioclase, clinopyroxene, olivine (altered to smectite), iron-titanium oxides, and sulfides are the main primary matrix phases. Glass is always present but is usually devitrified or altered. Vesicles and amygdules are variable in distribution and size, and most are filled with brown smectite and carbonate. In addition, plagioclase may be altered to light brown smectite.

The six dikes that cut lithologic Unit 14 can be subdivided into the following two groups: the first with the phenocryst assemblage plagioclase, olivine, and clinopyroxene, the second with plagioclase and olivine only as phenocrysts.

BASALT CHEMISTRY

Following previous compositional studies of drilled oceanic basalt (e.g., Flower et al., 1977; 1978; Byerly and Wright, in press), we have normalized major element analyses to a H_2O^+-free basis with total iron oxide expressed as FeO, assuming all water to be post-magmatic. A correction for added carbonate (mostly as $CaCO_3$ in veins and vugs) was made prior to normalization by subtracting a CO_2-equivalent CaO component from each analysis. Some corrected analyses show the effects of Ca^{+2} and Mg^{+2} leaching and enrichment in SiO_2 and K_2O. These appear to be the main changes in major element composition associated with smectite growth during sea-water percolation through the basalt pile. Empirical studies of fresh altered sample pairs from single cooling units (Flower et al., this volume) indicate that for both H_2O^+ and $K_2O < 0.20$ wt. per cent, leaching and addition effects are virtually negligible (except for K_2O and some trace elements). Hence, carbonate-corrected normalized analyses probably closely approximate original magmatic compositions.

Whole-rock compositional data for Holes 417D and 418A (Tables 3A and B) are used to define oxide variations, to make deductions about magmatic fractionation processes, and, by reference to lithologic and magnetic data, to refine stratigraphic divisions in the core. These divisions are further evaluated in light of the chemical alteration profiles at each drill site.

Stratigraphic Evaluation

Hole 417A

Shipboard analyses for Hole 417A reflect extreme alteration of the basalts (see Donnelly et al., this volume) with K_2O contents up to 6 wt. per cent and CaO contents less than 5 wt. per cent. Fresh material is rare or absent. The eight analyses listed in Table 1 were selected as the freshest available. These samples are from the lower part of the section (Cores 33 to 44) and suggest that original magma compositions in Hole 417A were indistinguishable from those in Hole 417D. However, the overall intensity of alteration in Hole 417A precludes detailed stratigraphic evaluation of magma chemistry. Magnetic stratigraphy is simple, with stable inclinations close to the predicted dipole.

Hole 417D

At Hole 417D, samples from each lithologic unit were analyzed. Except for the uppermost 2 to 3 meters of basement, alteration is slight and is concentrated along eruptive unit boundaries and in breccia zones. Stratigraphic boundaries of the eight glass compositional groups identified by Byerly and Sinton (this volume) are matched by changes in whole-rock composition (Figure 2). Chemical breaks illustrated by parameters such as TiO_2/Al_2O_3 ratios (reflecting fractionation of plagioclase) and $Mg/(Mg + Fe^{+2})$ ratios (reflecting fractionation of mafic phases) also commonly correlate with lithologic and stable magnetic unit boundaries (Figure 2). Because of this coincidence of chemical compositions with other parameters, the chemical data have been used to define an eruptive stratigraphy.

Theoretically, the products of a single eruption sampled by drilling should have: (1) uniform glass compositions, (2) whole-rock compositional variability consistent with effects of post-eruption fractionation, (3) uniform magnetic polarities and stable inclinations, (4) lithology consistent with the chemical data, and (5) no major sedimentary or clastic intercalations. In practice, however, the chemical, lithologic, and magnetic character of single eruptive units can undergo considerable variation. Variations in glass compositions can arise from nonhomogeneities in the sub-rift magma chamber, and whole-rock compositions can reflect extensive phenocryst redistribution and post-eruptive crystallization. Stable magnetic inclinations can reflect differential subsidence and rotation of crustal blocks during a single eruption, and lithologies can vary markedly as a result of

TABLE 2
DSDP Numbers Corresponding to Those of the Bochum Laboratory and Computer File for Samples Analyzed

Bochum Number	DSDP Sample Number (Interval in cm)	Piece Number
Hole 417A		
110	33-5, 54-58	5A
120	34-2, 88-93	8A
160	37-1, 37-40	1B
180	38-3, 75-79	10
210	40-3, 25-29	1
220	41-3, 92-97	2
240	44-2, 13-17	1A
250	44-3, 58-68	9
Hole 417D		
1010	–	–
1020	22-4, 24-28	1A
1040	22-6, 143-148	8
1060	26-6, 87-91	4B
1080	28-1, 44-50	3A
1110	28-6, 111-117	4
1120	29-2, 50-54	3
1140	29-6, 8-13	1A
1150	30-2, 82-86	2A
1170	30-7, 90-96	3
1180	31-2, 98-102	2F
1185	31-4, 78-80	3A
1210	33-4, 47-52	3B
1240	35-4, 27-33	3A
1275	36-3, 127-129	6
1280	36-4, 36-39	2A
1300	–	–
1320	38-4, 106-111	5A
1330	39-3, 95-101	2
1400	42-1, 10-16	1B
1440	43-3, 52-57	1D
1460	44-1, 54-59	3A
1480	45-1, 5-8	1A
1500	48-6, 113-115	4C
1510	49-1, 109-111	8B
1520	49-3, 55-57	4
1530	50-2, 73-75	2
1540	52-3, 87-89	1F
1550	52-5, 20-22	2
1560	53-2, 109-111	7
1570	54-1, 89-91	6
1580	54-6, 21-23	1B
1590	55-2, 7-9	1
1600	55-4, 110-112	6
1620	57-2, 62-64	7B
1630	57-3, 44-46	4B
1640	58-1, 127-129	10
1650	59-1, 121-123	8
1660	59-5, 82-84	6
1670	60-3, 109-111	6B
1690	62-4, 36-38	4
1710	63-3, 105-107	10
1720	64-1, 53-55	2
1730	65-1, 111-113	10
1740	65-5, 23-25	2
1750	67-1, 56-58	1F
1760	67-2, 71-73	10
1780	68-5, 83-85	3
1790	69-2, 9-11	1
Hole 418A		
10	15-1, 27-29	2A
15	15-1, 124-127	1L
20	15-2, 52-56	5B
30	16-1, 72-74	2B
40	17-1, 134-139	3C
50	17-3, 124-126	1I
55	18-1, 66-68	2E
60	18-2, 33-38	2A
70	18-2, 99-123	3C
80	18-4, 26-29	1A
90	18-6, 89-94	3B
100	19-2, 57-61	1C
103	19-3, 66-68	1D
106	19-6, 100-102	3F
110	20-1, 103-108	6F
120	20-2, 68-73	1G
130	20-3, 49-54	1G
133	20-4, 7-9	1A
136	20-5, 40-42	2A
140	20-7, 101-104	3
146	22-1, 129-131	11B
150	22-2, 55-59	1G
152	23-1, 22-26	2
154	24-1, 103-105	3B
156	24-2, 71-74	4
158	25-1, 36-38	2
160	25-2, 145-148	5G
170	26-1, 16-20	1A
180	26-2, 76-80	2D
190	26-4, 144-147	–
193	27-1, 24-26	–
195	27-1, 133-135	–
197	27-2, 83-85	–
215	28-2, 130-132	10B
220	28-4, 20-24	1B
225	28-5, 11-13	1
230	29-1, 97-100	8
245	30-2, 124-126	6B
248	31-1, 98-100	6
250	31-3, 103-106	11
260	33-1, 75-78	–
266	33-2, 85-87	6A
270	33-4, 105-108	6B
280	33-4, 136-139	6E
286	33-6, 59-61	5A
290	34-1, 89-93	2F
292	34-4, 15-17	1B
294	35-1, 21-23	3A
300	35-4, 93-99	3F
303	36-1, 100-103	8C
310	36-3, 80-84	3D
320	36-5, 136-139	–
330	38-1, 75-78	3B
340	38-3, 128-130	7
342	38-4, 77-79	5A
346	39-2, 13-15	1
348	40-2, 59-61	2D
350	40-2, 85-88	3A
355	41-1, 32-34	4A
360	41-1, 100-104	7
370	42-1, 52-54	2E
375	42-2, 81-83	6
380	42-3, 11-15	1A
395	42-3, 51-53	3
400	42-4, 9-12	1A
420	42-5, 27-30	2
425	42-5, 65-67	5
430	43-1, 78-80	4D
435	43-1, 109-111	8D
440	43-1, 136-140	5B
450	44-3, 29-32	3
460	44-3, 104-106	6B
462	44-5, 42-44	3A

TABLE 2 – *Continued*

Bochum Number	DSDP Sample Number (Interval in cm)	Piece Number
464	45-1, 73-75	5C
470	45-3, 22-26	1B
490	46-1, 25-30	2A
500	46-2, 77-81	4A
510	46-3, 126-134	8B
520	46-4, 31-36	3B
530	47-2, 93-98	4A
540	47-2, 123-126	2D
550	47-5, 102-105	5
570	48-1, 136-142	5G
575	48-3, 50-52	3A
580	48-3, 73-78	3G
590	48-4, 21-24	2G
595	48-0, 70-72	2
600	49-1, 61-65	3G
610	49-1, 135-139	6E
620	49-2, 27-30	1G
630	50-2, 49-53	3A
640	50-3, 131-133	2H
650	50-4, 42-45	4A
660	50-5, 47-50	3A
670	51-2, 13-16	1A
680	51-3, 122-126	6B
690	51-4, 57-60	3G
700	51-5, 21-26	2
720	52-1, 122-125	10
730	53-1, 108-113	9
740	53-2, 128-130	6B
750	55-3, 125-128	8
760	55-4, 142-145	12
770	56-1, 116-119	6B
780	56-4, 21-24	1B
790	56-7, 22-26	2
800	56-7, 69-74	–
810	60-1, 27-30	1G
820	60-4, 144-148	1M
830	61-1, 15-18	1
840	62-4, 3-8	1A
850	63-2, 103-109	4A
860	63-2, 126-130	4B
870	64-4, 77-81	2E
880	65-1, 139-140	8
890	65-3, 21-26	2
900	65-4, 110-113	5D
910	65-5, 22-26	1G
920	66-3, 29-34	2
940	66-6, 127-131	8A
950	68-1, 44-48	2G
960	68-1, 65-70	2E
970	69-1, 134-140	2C
980	69-6, 24-28	2A
990	69-6, 124-129	4B
1010	70-5, 40-44	2G
1040	71-2, 23-26	1D
1060	72-2, 89-94	3G
1070	72-3, 23-28	1B
1080	72-3, 130-134	5
1090	73-3, 2-9	1
1100	73-3, 43-46	3A
1110	73-4, 124-129	2G
1130	74-2, 48-120	3A
1140	74-3, 120-126	1
1160	76-3, 89-92	1G
1170	77-4, 133-136	2E
1180	78-3, 96-99	2D
1190	79-3, 42-118	1I
1200	79-4, 18-22	1C
1210	79-4, 140-143	2G
1220	80-2, 46-49	2

TABLE 2 – *Continued*

Bochum Number	DSDP Sample Number (Interval in cm)	Piece Number
1230	80-2, 132-134	7
1240	80-3, 48-52	2
1250	80-5, 35-39	1C
1260	80-6, 47-120	6B
1270	82-1, 35-37	–
1280	83-1, 15-19	1B
1290	84-2, 43-38	1C
1300	85-1, 14-18	1
1310	85-2, 80-84	4
1320	85-6, 29-32	3C
1330	85-7, 97-101	5
1340	86-1, 2-6	1A
1350	86-2, 33-37	3
1360	86-2, 47-50	4A
1370	86-2, 66-69	4B
1380	86-3, 100-112	7
1400	86-4, 38-42	1D
1410	86-4, 48-124	7A

different eruptive rates and variable rift topography. We believe that glass compositions and magnetic inclinations are least likely to vary significantly during a single eruption. Consequently, we have defined eruptive units as stratigraphic sequences bounded by both chemical and magnetic breaks and, accordingly, have identified a maximum of 25 and a minimum of 13 eruptive units for the section penetrated at Hole 417D. The number of eruptive units may be underestimated because of difficulty in interpretation of the breccias and the possibility that different eruptions are chemically and magnetically indistinguishable. Alternatively, the number of units may be overestimated if intra-eruption variation is greater than we have assumed. The eruptive units vary in thickness from 1 meter to about 60 meters, but because sampling by a single drill hole is unrepresentative, these thicknesses probably do not reflect original eruptive volumes.

These eruptive units can be grouped into at least three major sequences bounded by major stratigraphic discontinuities (Figure 2). The discontinuities are believed to be major eruptive breaks as evidenced by marked changes in basalt composition and magnetic inclinations, and often by the presence of breccia zones and altered horizons.

Hole 418A

All 16 lithologic units in Hole 418A were sampled for analysis. As in Hole 417D, glass groupings (Byerly and Sinton, this volume) complement whole-rock compositions and, when combined with magnetic inclinations, permit a detailed breakdown of the eruptive record (Figure 3). Byerly and Sinton (this volume) infer 11 stratigraphic glass groups and define a separate group for the dikes traversing lithologic Unit 14C. The glass groups correspond well with the lithologic and magnetic units (Figure 3), but can be further divided on the basis of whole-rock variations of TiO_2/Al_2O_3 ratios and $Mg/(Mg + Fe^{+2})$ ratios. Using the same criteria as for Hole 417D, we infer a maximum of 54 and a minimum of 32 eruptive units for the Hole 418A section, not including the dikes (Figure 3). Downhole magnetic and chemical discontinuities are more numerous and

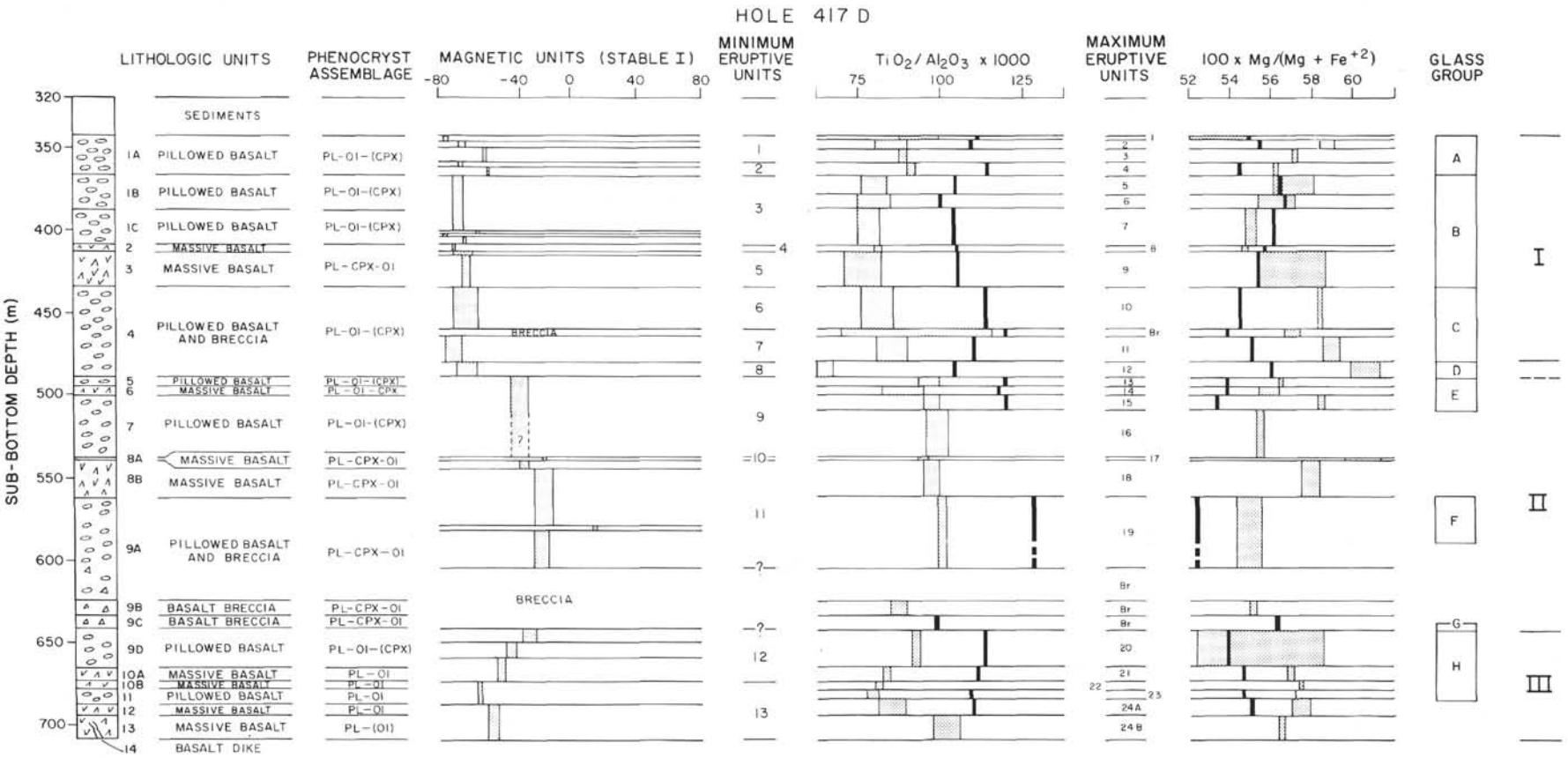

Figure 2. *Hole 417D, summary of lithologic, magnetic, and chemical stratigraphy. Lithologic units are updated shipboard core divisions. Magnetic units are based on stable inclination variations measured onboard; the average Cretaceous dipole was ±38°. Eruptive units are interpreted from downhole chemical and magnetic variations; average glass compositions (thick vertical lines) are shown in comparison to the range of whole-rock compositions for each eruptive unit in terms of* TiO_2/Al_2O_3 *and* $Mg/(Mg + Fe^{+2})$ *ratios. Glass composition groups are after Byerly and Sinton (this volume): BR = breccia. Note: MgO and FeO in eruptive Unit 1 reflect a high degree of alteration.*

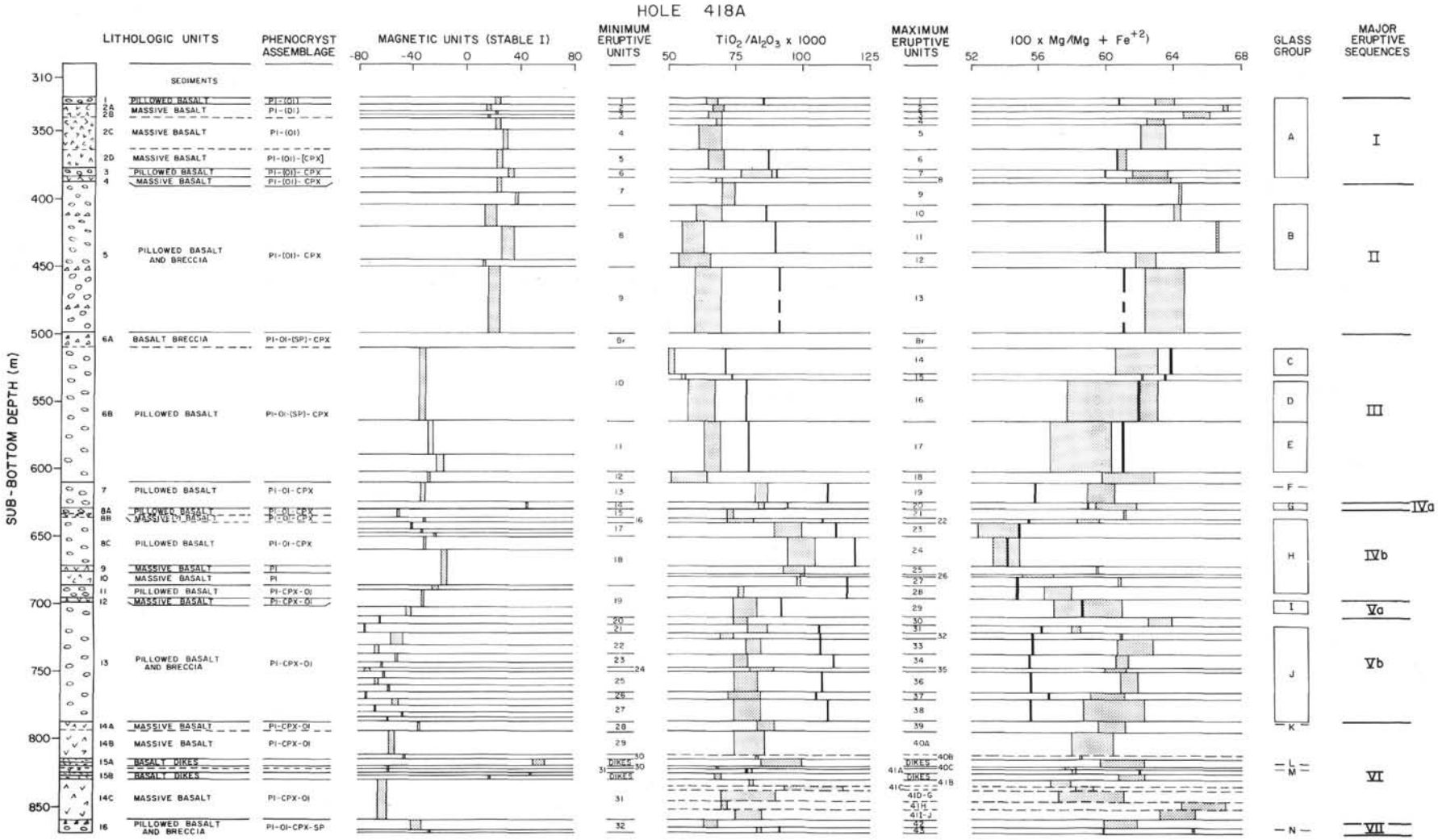

Figure 3. *Hole 418A, summary of lithologic, magnetic, and chemical stratigraphy. The lithologic units are updated shipboard core divisions. Magnetic units are based on stable inclination variations measured on board. Eruptive units are interpreted from downhole chemical and magnetic variations; average glass compositions (thick vertical lines) are shown in comparison to the range of whole-rock compositions for each eruptive unit in terms of* TiO_2/Al_2O_3 *and* $Mg/(Mg + Fe^{+2})$ *ratios. Glass compositional groups are after Byerly and Sinton (this volume).*

TABLE 3A
Whole-Rock Compositional Averages for Eruptive Units at Hole 417D, Based on Fresh, Carbonate-Corrected Analyses (see text)

Unit No.	2	5	6	7	8	9	10	BR[a]	11	12	13	14	16	17	18	19	20	21	22	23	24A	24B	X[b]
SiO_2	50.15	50.15	50.71	50.61	50.43	50.46	49.83	50.13	49.70	50.46	50.21	50.48	50.23	50.78	51.08	50.06	50.47	50.64	49.81	50.25	50.34	50.62	49.45
Al_2O_3	17.10	17.52	17.54	17.78	17.60	17.32	17.40	16.72	16.93	17.67	16.01	16.04	16.64	16.62	15.43	15.53	15.98	16.39	16.63	17.13	16.32	15.37	22.52
"FeO"	9.71	9.40	9.13	9.40	9.50	9.48	9.45	9.97	9.50	8.72	10.43	10.36	10.51	9.08	10.09	10.95	10.32	9.84	10.12	9.56	9.93	10.63	7.38
MgO	7.05	6.31	5.85	5.77	5.77	6.07	6.75	6.69	6.86	6.68	6.81	6.65	6.58	7.02	7.02	6.67	6.41	6.57	6.95	6.12	6.84	6.94	5.32
CaO	11.96	12.69	13.00	12.38	12.63	12.54	12.55	12.60	12.58	13.15	12.30	12.30	11.77	12.37	12.36	12.61	12.71	12.80	12.75	13.22	12.82	12.26	12.86
Na_2O	2.39	2.37	2.32	2.28	2.45	2.49	2.44	2.29	2.79	2.04	2.57	2.51	2.11	2.50	2.46	2.54	2.55	2.36	2.31	2.33	2.34	2.58	1.48
K_2O	0.07	0.06	0.04	0.13	0.18	0.09	0.06	0.04	0.06	0.03	0.07	0.13	0.21	0.07	0.06	0.07	0.04	0.02	0.05	0.02	0.03	0.04	0.06
TiO_2	1.46	1.39	1.40	1.41	1.44	1.42	1.40	1.39	1.38	1.16	1.60	1.53	1.58	1.56	1.49	1.57	1.53	1.38	1.36	1.37	1.37	1.56	0.93
P_2O_5	0.05	0.06	0.00	0.13	0.00	0.06	0.06	0.08	0.08	0.05	0.00	0.00	0.17	0.00	0.00	0.00	0.00	0.00	0.00	0.00	0.00	0.00	0.00
MnO	0.06	0.06	0.00	0.11	0.00	0.06	0.06	0.08	0.11	0.05	0.00	0.00	0.20	0.00	0.00	0.00	0.00	0.00	0.00	0.00	0.00	0.00	0.00

[a]BR = breccia.
[b]X = dike.

TABLE 3B
Whole-Rock Compositional Averages for Maximum Eruptive Units at Hole 418A, Based on Fresh, Carbonate-Corrected Analyses (see text)

Unit No.	1	2	3	4	5	6	7	8	9	10	11	12	13	BR[a]	14	15	16	17	18	19
SiO_2	50.58	51.36	50.60	50.39	50.19	50.86	50.58	50.40	50.29	50.51	50.46	49.97	49.98	49.98	49.70	49.68	49.85	49.74	49.78	50.11
Al_2O_3	17.34	18.24	17.83	16.72	16.95	16.49	15.88	16.85	18.52	18.84	19.79	18.14	18.15	18.61	18.46	19.38	17.63	17.97	17.98	15.85
"FeO"	8.78	7.74	8.21	9.22	8.99	9.22	9.47	9.10	8.32	7.96	7.24	8.67	8.42	8.86	8.37	7.98	9.14	9.21	8.79	10.22
MgO	7.36	7.33	7.15	7.41	7.22	7.12	7.64	7.09	7.11	6.70	6.60	6.81	6.80	5.52	6.39	6.12	6.74	6.15	6.67	7.32
CaO	12.44	11.63	12.32	12.60	12.91	12.92	12.62	12.84	12.08	12.07	12.75	12.87	12.94	13.70	13.56	12.92	13.05	13.31	13.19	12.56
Na_2O	2.24	2.32	2.42	2.28	2.27	2.12	2.36	2.30	2.32	2.42	2.03	2.18	2.28	2.08	2.23	2.40	2.23	2.22	2.23	2.26
K_2O	0.05	0.09	0.12	0.07	0.09	0.05	0.04	0.10	0.07	0.15	0.06	0.08	0.06	0.16	0.08	0.18	0.08	0.06	0.05	0.04
TiO_2	1.14	1.29	1.18	1.13	1.10	1.14	1.32	1.15	1.29	1.19	1.07	1.14	1.23	1.09	0.99	1.09	1.08	1.09	0.99	1.34
P_2O_5	0.03	0.00	0.08	0.07	0.10	0.03	0.04	0.07	0.00	0.05	0.00	0.05	0.04	0.00	0.09	0.10	0.07	0.09	0.14	0.12
MnO	0.04	0.00	0.08	0.11	0.17	0.05	0.05	0.09	0.00	0.11	0.00	0.08	0.08	0.00	0.13	0.15	0.13	0.15	0.17	0.18

[a]BR = breccia.
[b]X and Y are probable dikes.

TABLE 3B – *Continued*

Unit No.	20	21	22	23	24	25	26	27	28	29	30	BR[a]	31	32	33	34	35	36	37	38
SiO_2	50.17	49.62	49.69	50.17	49.21	49.63	50.38	50.03	49.01	49.51	50.19	49.64	49.52	49.61	50.06	49.65	50.52	49.89	50.03	49.97
Al_2O_3	15.82	17.17	17.19	16.34	16.16	16.78	15.53	16.27	16.89	16.32	17.52	17.66	16.69	16.81	16.10	16.41	15.65	16.05	16.09	16.53
"FeO"	9.79	9.19	9.46	10.40	11.11	10.21	10.88	9.94	10.37	9.98	8.59	8.99	10.03	9.60	9.85	9.78	9.95	9.84	9.88	9.64
MgO	7.47	7.16	6.84	6.09	6.58	7.31	6.85	7.46	6.51	7.02	7.00	6.76	6.81	7.24	7.36	7.38	7.48	7.45	7.28	7.28
CaO	12.72	12.93	12.80	12.72	12.46	11.82	11.96	11.65	12.93	13.03	12.48	12.67	12.90	12.84	12.64	12.94	12.35	12.82	12.77	12.60
Na_2O	2.35	2.33	2.32	2.34	2.43	2.33	2.44	2.58	2.42	2.36	2.49	2.61	2.28	2.30	2.30	2.23	2.30	2.25	2.28	2.28
K_2O	0.05	0.04	0.06	0.09	0.09	0.04	0.09	0.11	0.06	0.17	0.04	0.04	0.07	0.04	0.06	0.05	0.08	0.06	0.09	0.06
TiO_2	1.32	1.26	1.35	1.49	1.61	1.58	1.56	1.60	1.48	1.30	1.34	1.34	1.37	1.25	1.30	1.25	1.34	1.30	1.28	1.30
P_2O_5	0.13	0.13	0.13	0.20	0.16	0.14	0.13	0.16	0.14	0.14	0.18	0.14	0.13	0.13	0.13	0.13	0.13	0.13	0.13	0.13
MnO	0.19	0.17	0.17	0.17	0.19	0.16	0.18	0.20	0.18	0.16	0.16	0.15	0.20	0.18	0.19	0.18	0.19	0.20	0.17	0.20

TABLE 3B – *Continued*

Unit No.	39	40A	40B	40C	41A	41B	41C	41D	41E	41F	41H	41I	41J	42	43	X[b] 2	X 3	Y[b] 1	Y3
SiO_2	50.30	50.78	50.98	50.54	50.32	50.39	50.64	50.43	50.26	49.80	49.60	50.27	49.84	49.67	50.25	50.35	50.09	49.77	49.61
Al_2O_3	16.36	15.98	15.92	17.05	16.52	16.42	14.39	15.51	15.97	16.72	15.92	15.87	15.79	17.90	16.07	14.68	16.05	17.26	17.57
"FeO"	9.83	9.69	9.66	9.50	9.91	9.96	10.93	10.40	9.96	9.77	9.71	9.65	9.54	8.87	9.18	11.09	9.83	9.23	9.08
MgO	7.22	6.76	6.57	6.30	6.67	6.56	7.64	7.37	7.37	7.21	9.04	8.10	8.40	6.70	8.24	8.09	7.44	7.08	7.02
CaO	12.06	12.84	12.87	12.83	12.58	12.67	12.12	12.20	12.60	12.71	12.14	12.29	12.35	13.07	12.10	11.69	12.59	12.97	12.98
Na_2O	2.53	2.29	2.31	2.25	2.30	2.31	2.38	2.31	2.25	2.28	2.11	2.23	2.34	2.23	2.37	2.29	2.32	2.21	2.27
K_2O	0.07	0.05	0.03	0.04	0.05	0.04	0.03	0.07	0.03	0.04	0.06	0.04	0.10	0.07	0.13	0.03	0.04	0.03	0.03
TiO_2	1.33	1.30	1.32	1.20	1.33	1.35	1.55	1.41	1.29	1.19	1.13	1.24	1.31	1.19	1.34	1.47	1.35	1.19	1.14
P_2O_5	0.12	0.14	0.14	0.13	0.15	0.13	0.13	0.13	0.10	0.12	0.11	0.14	0.12	0.13	0.14	0.13	0.13	0.10	0.13
MnO	0.18	0.17	0.20	0.16	0.17	0.17	0.19	0.18	0.17	0.16	0.17	0.17	0.20	0.18	0.17	0.19	0.17	0.16	0.17

more pronounced than in Hole 417D, but the greater abundance of chemical and magnetic data for this hole also allows more precise definition of the eruptive history.

In the Hole 418A sequence we recognize seven major eruptive sequences bounded by stratigraphic breaks. Most of the recognized stratigraphic breaks are characterized by zones of higher alteration and three of them are marked by magnetic polarity reversals. Stable magnetic inclination changes occur both at and between the major stratigraphic breaks.

COMPOSITIONAL VARIATIONS OF BASALT MAGMAS

Byerly and Sinton (this volume) conclude from glass compositional variation that shallow-level crystal fractionation accounts for most observed variations in liquid compo-

sitions, but that multiple parent liquids may be required to account for the total variation. We are not yet able to give a definitive account of fractionation relationships, since this requires comprehensive treatment of our data. However, we can use average compositions for each chemical unit to summarize variation features and to point to the most likely fractionation processes.

Figures 4a,b and 5a,b show average (corrected) compositions of each eruptive unit plotted in terms of MgO and Al_2O_3 versus TiO_2. Each composition is classified according to the glass group defined by Byerly and Sinton (this volume) with which they are associated in the core. Whole-rock compositions clearly do not follow a single fractionation path and if, as appears likely, the glasses are restricted

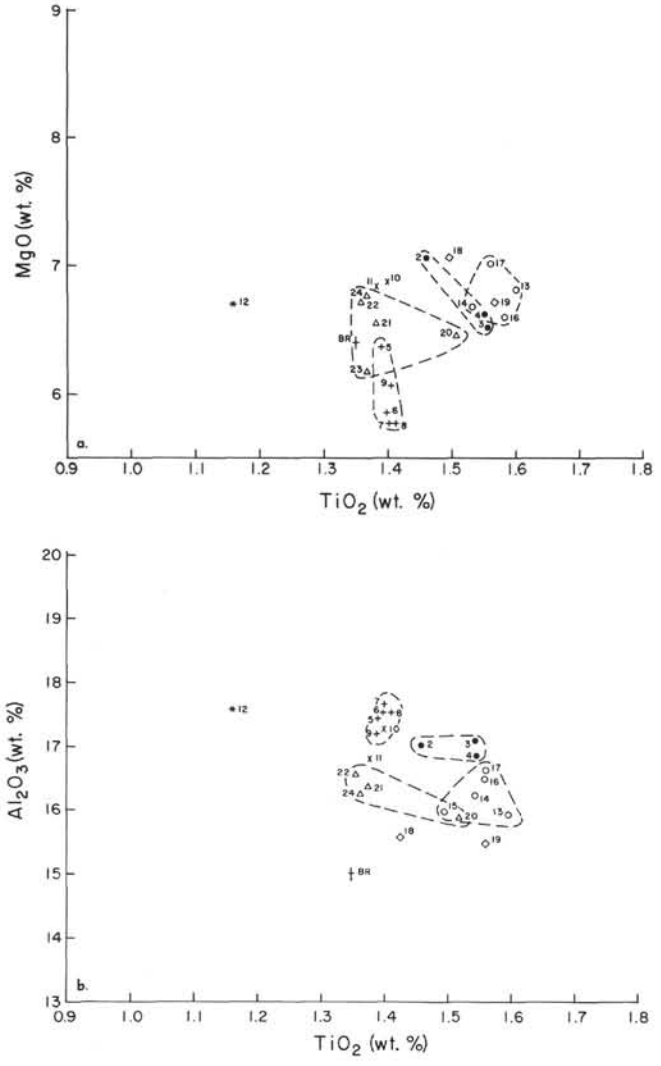

Figure 4. *MgO and Al_2O_3 versus TiO_2 for Hole 417D; (a) MgO versus TiO, and (b) Al_2O_3 versus TiO_2. Whole-rock average compositions for maximum eruptives units are identified according to the associated glass compositional groups (Byerly and Sinton, this volume). Glass group symbols: Hole 417D -A ●; -B +; -C x; -D *; -E o; -F ◇; -G †; -H △. Units 1 and 15 are defined on glass compositions alone.*

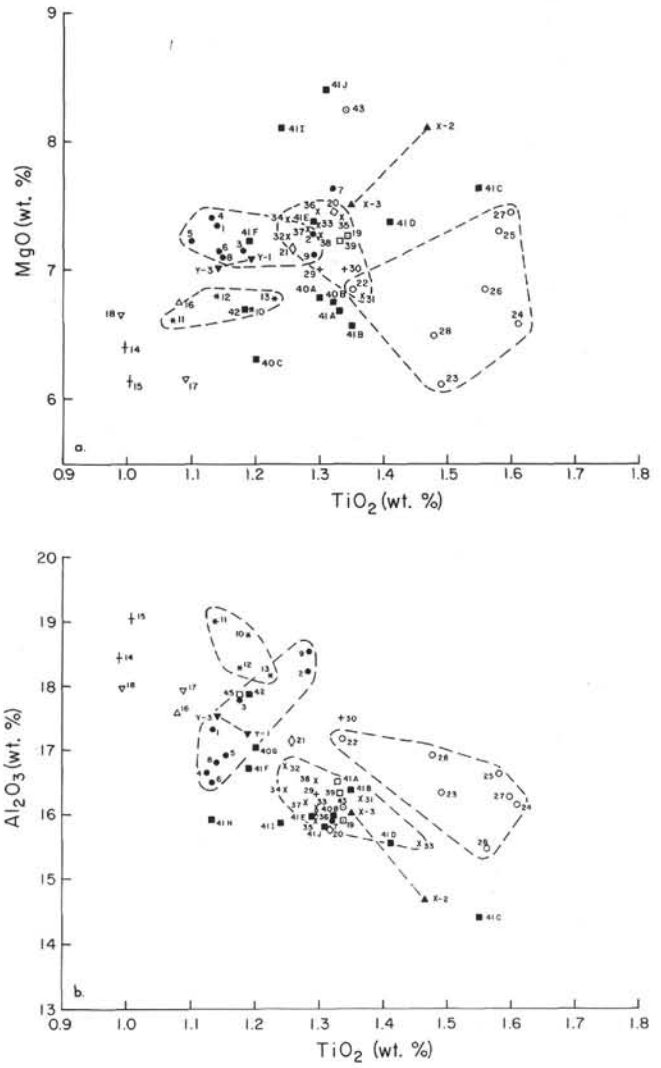

Figure 5. *MgO and Al_2O_3 versus TiO_2 for Hole 418A; (a) MgO versus TiO_2, and (b) Al_2O_3 versus TiO_2. Average compositions for maximum eruptive units are identified according to glass compositional groups (Byerly and Sinton, this volume). Glass group symbols: Hole 418A -A ●; -B *; -C †; -D △; -E △; -F □; -G ◇; -H o; -I +; -J x; -K □; -L (dike, x-type ▲); -L (dike, y-type ▲); -M ■); -N ○.*

to a single line of liquid descent, whole-rock variation must result from differential phenocryst movement during and after a major crystallization stage at depth. The variation pattern thus reflects the unique modal mineralogy and fractionation history of any single eruption.

The comparatively low values of $Mg/(Mg + Fe^{+2})$ (0.50 to 0.65) and TiO_2/Al_2O_3 (0.070 to 0.120) in aphyric and sparsely phyric samples and the complex phenocryst assemblages of phyric basalts indicate that all of the lavas are evolved compared to primitive mantle melts. The liquid (glass) fraction conforms to a low-pressure three-phase cotectic crystallization trend (Byerly and Sinton, this volume) typical of ocean-floor tholeiite crustal fractionation.

Figures 2 and 3 show the downhole variations of whole-rock and associated glass compositions for individual eruptive units. TiO_2/Al_2O_3 variation shows the widespread ef-

fects of accumulated plagioclase in lavas at both sites. An exception appears to be lithologic Unit 14c in Hole 418A, a massive aphyric to sparsely phyric flow in which considerable internal fractionation seems to have occurred during and after outflow (Figure 3), with only few portions of the flow enriched in plagioclase.

In contrast to plagioclase, olivine and in some cases, early formed clinopyroxene, appear to have been in equilibrium or nearly so with the associated liquids ($K_D = XFeO^{ol}\ MgO^{liq}/XMgO^{ol}\ XFeO^{liq} = 0.33$) (see Flower et al., 1977). However, in certain eruptive units (e.g., Sections 417D-10-13, 418A-15-18, and 418A-45-46) early formed clinopyroxene appears to coexist metastably with spinel and shows a reaction relation with the liquid phase.

The discrepancy in $Mg/(Mg + Fe^{+2})$ ratios for whole-rock and glass compositions (Figures 2 and 3) suggests a more complex role for mafic phases during fractionation than for plagioclase. Whereas TiO_2/Al_2O_3 ratios for whole-rock compositions are mostly lower than those of associated glasses, whole-rock $Mg/(Mg + Fe^{+2})$ ratios may be greater, less than, or equal to the glass values (Figures 2 and 3). These relationships suggest some degree of decoupling between mafic and feldspathic crystals, and possibly between olivine and clinopyroxene crystals, during the fractionation process. Another possible explanation is the development of iron-rich smectite in the crystalline rocks (cf., Byerly and Wright, in press). Although a majority of eruptive units at both sites show higher $Mg/(Mg + Fe^{+2})$ ratios for whole-rock compositions than for glass, there are several notable exceptions (e.g., units 15 through 18 in Hole 418A).

Because any single glass compositional group may include more than one eruptive unit, we assume that differences in liquid-fraction composition of magmas are largely the result of pre-eruption fractionation. Phenocrysts appear to be exclusively of low-pressure origin, so that fractionation probably comprised protracted crystallization under relatively steady conditions coupled with gravity separation of the crystal-liquid fractions. In theory, if eruption rates are sufficiently high, so that no further crystallization occurs during eruption, the liquid fraction should be in equilibrium with the pre-eruptive crystalline phases. Further crystallization of phenocrysts or microphenocrysts after eruption would coincide with rapid chilling of the liquid fraction, resulting in negligible compositional changes. Hence, in either case, glass compositions should be relatively uniform over discrete core intervals, assuming that the magma chamber was not compositionally zoned or that mixing of fractionated and primitive magmas did not occur during eruption. Phenocryst redistribution during and after eruption probably accounts for much of the discrepancy between glass and whole-rock compositions, especially where whole-rock $Mg/(Mg + Fe^{+2})$ ratios exceed those of glass. However, the widespread occurrence of accumulated plagioclase suggests this is the result of temporary magma arrest at depth in reservoirs permitting massive flotation of this phase.

Trace-element studies generally confirm the findings from major elements. Plots of alteration-resistant lithophile elements Zr, Y, and Ti are shown in Figures 6a and 6b as average values for Hole 418A eruptive units, identified according to the associated glass groups (Byerly and Sinton,

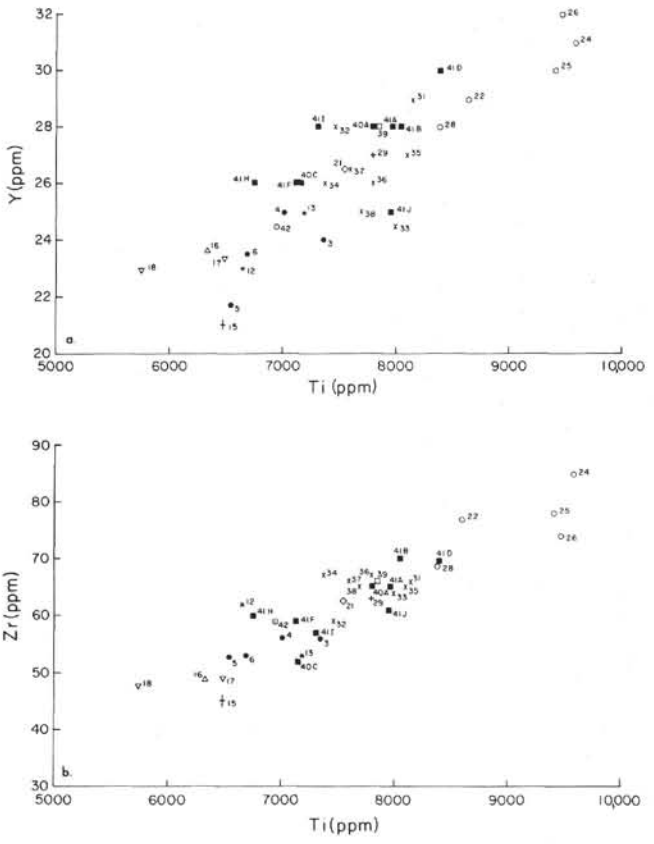

Figure 6. *Y and Zr versus Ti for Hole 418A; (a) Y versus Ti (ppm), and (b) Zr versus Ti (ppm). Average compositions for maximum eruptive units are identified according to glass compositional groups; symbols as in Figure 5.*

this volume). Zr and Y versus Ti exhibit positive linear patterns of essentially constant interelement ratios ($Zr/Y = 2.1$ to 2.4; $Ti/Y = 273$ to 297; $Ti/Zr = 121$ to 133) and show no significant differences between chemical groups. Differences in abundance of these elements can probably be attributed to fractional crystallization and/or crystal accumulation, because enrichment factors (1.5 to 1.6) are no greater than would be expected for the range of major element variation. Multiple primary magma batches would be required if the variation could not be modeled by fractional crystallization of the observed (or postulated) liquidus phases. As a tentative conclusion we suggest that parental magmas at Holes 417D and 418A were similar in composition, but may nonetheless have shown subtle differences between consecutive batches.

STRATIGRAPHIC SUMMARY

Stratigraphic sections at both Holes 417D and 418A show sharp chemical and lithologic discontinuities accompanied by changes in stable magnetic inclination and sometimes in polarity. However, core intervals between major discontinuities also often show significant secular changes in both basalt compositions and stable magnetic inclinations (Figures 2 and 3). Good examples are eruptive sequences I, II, IV, and V in Hole 418A and sequences II and III in Hole 417D. Some of these intervals show an upward transition

from evolved to less-evolved compositions corresponding in certain cases to progressive changes in stable inclinations. Such patterns appear to reflect cyclic activity during crustal formation. A single cycle appears to comprise a sequence of several eruptions from the same conduit system. Succeeding cycles may tap completely new conduit systems depending on the duration of the preceding quiescent period and the crustal spreading rate (see Flower et al., 1977). The pattern of magnetic inclinations observed may thus reflect a systematic regime of tectonic deformation accompanying eruptive episodes, and indicate subsidence due to lateral spreading and the exhaustion of temporary magma reservoirs. If this interpretation is correct, inclinations of the uppermost flows in a newly active cycle should show the smallest departure from dipole values assuming deposition was horizontal. Initiation of a new cycle from a separate system should result in nonconformable deposition of new lavas and further (although to a progressively lesser extent) tilting of the underlying pile.

The downhole magnetic-inclination pattern transgresses the dipole average value seven times in Hole 418A and four times in Hole 417D, showing that "aberrant" stable inclinations are not exclusively high or low. This may indicate oscillatory movement of the spreading axis in which crustal build-up proceeds with sequential eruptive episodes and interim periods of tilting with lateral movement whose direction is only established unambiguously on final completion of the pile. Such a process is consistent with the decrease in variability of inclination towards the top of Holes 418A and 417D, although in the latter the inclinations are consistently higher than dipole values (Figures 2 and 3). In either case, the lithologic, chemical, and magnetic stratigraphy becomes simpler as this segment of crust evidently became finally committed to the western spreading limb.

The alteration profiles at Holes 417D and 418A provide further evidence for episodic eruption. A strong repetitive downhole pattern is shown by K_2O, and to a lesser extent, by H_2O^+, reflecting mainly oxidative alteration to produce K-rich smectite. This is most concentrated at and below depositional surfaces of "exposed" lava sequences delineated by the major stratigraphic breaks (Figures 7a and 7b). Above many of these horizons a comparatively sharp drop occurs in K_2O and H_2O^+. Minor variants of this pattern are also present, suggesting several lesser gaps in the eruptive record.

In both sections the episodic pattern is superimposed on an overall downhole decrease in oxidation and H_2O^+ content based on data from flow interiors and from lower, less altered, parts of individual cyclic intervals (Figures 7a and 7b). This "pervasive" alteration gradient appears to terminate at a depth of about 850 meters, where contents of H_2O^+ and K_2O are effectively juvenile. The increasing freshness with depth of drilled basement — especially of glass and groundmass minerals such as olivine — was one of the major surprises resulting from drilling of Cretaceous crust. Presumably, typical crust of this age is mostly fresh below about 500 meters sub-basement depth, and is altered only during short-lived periods of exposure to sea water between eruptive episodes and prior to sediment deposition. On the assumption that time gaps between major eruptive sequences are of the same approximate length, the downhole decrease in alteration must reflect a sharp decline in circulation of sea water through the basaltic crust as it moves away from the spreading axis. We conclude that crust at Holes 417D and 418A (but not Hole 417A) was effectively sealed soon after construction, possibly by sedimentation, and that circulating water was progressively restricted to shallower levels as its availability declined and hydrous alteration phases formed in the pile.

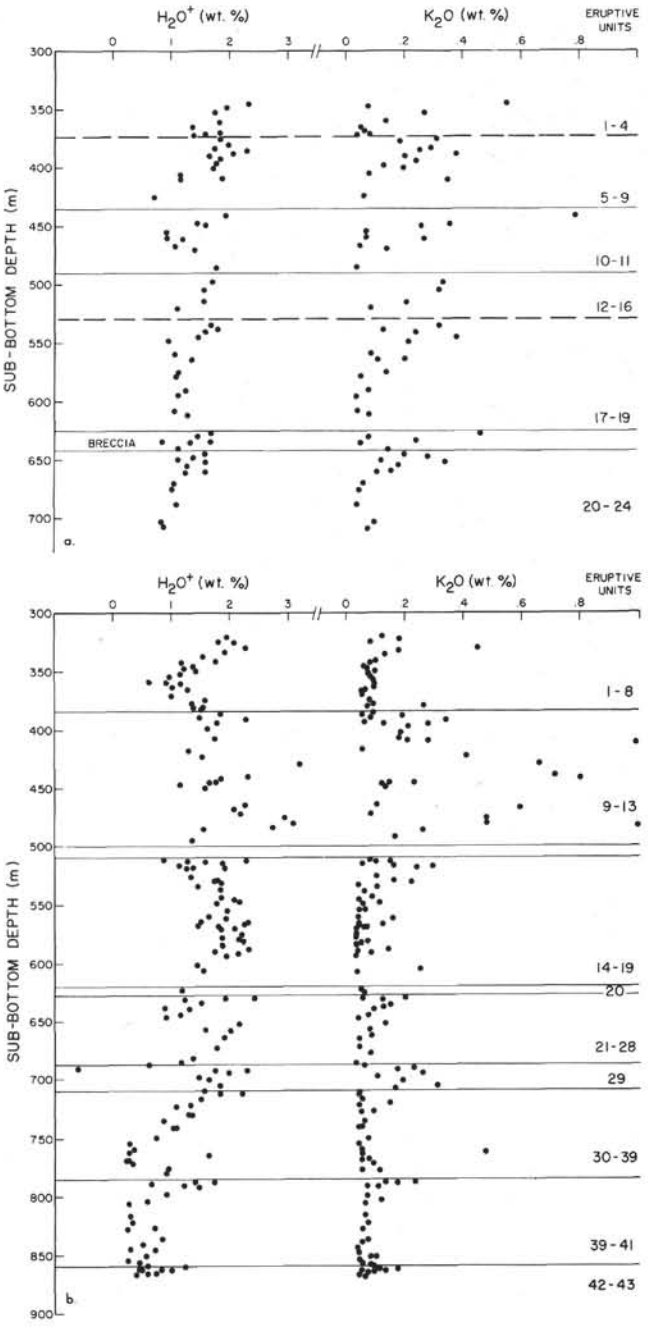

Figure 7. *Plots of H_2O and K_2O versus sub-bottom depth. Horizontal lines show major stratigraphic breaks, dashed lines subsidiary breaks; (a) Hole 417D, and (b) Hole 418A.*

CONCLUSIONS

In contrast to previous attempts at basement drilling in the Atlantic Ocean, deep penetration and excellent recovery at Sites 417 and 418 allow detailed reconstruction of the erup-

tive stratigraphy. The main conclusions from study of Holes 417D and 418A may be summarized as follows:

1) Eruptive crust was probably built up by a number of small eruptions, each characterized by flows of relatively uniform composition and stable magnetic inclinations.

2) At both sites larger scale eruptive cycles apparently reflect draining of separate high-level magma chambers. Generally, the boundaries between these large cycles are marked by lithologic, chemical, and magnetic breaks in the core.

3) The resulting pattern of chemical stratigraphy is matched by variable stable magnetic inclinations suggesting that eruptive episodes undergo progressive tectonic deformation, possibly in the context of an oscillating spreading axis.

4) Downhole alteration profiles reflect rapid crustal sealing, probably by sedimentation and growth of secondary phases, causing reduced permeability. Zones of intense oxidative alteration coincide generally with noneruptive periods.

5) In contrast to the modern Mid-Atlantic Ridge at 22°N and 37°N, the inferred chemistry of primary magma batches at Sites 417 and 418 reflects comparatively uniform conditions of partial melting and source composition.

6) Compositional variations in the erupted basalts are probably due largely to crystal fractionation and post-eruption phenocryst redistribution.

ACKNOWLEDGMENTS

The manuscript was read critically by Tom L. Wright.

REFERENCES

Abbey, S., 1973. Studies in "standard samples" of silicate rocks and minerals. Part 3. 1973 extension and revision of "usable" tables, *Canadian Geol. Publ.*, p. 1-24.

Byerly, G. and Wright, T. L., in press. Origin of major element chemical trends in DSDP Leg 37 basalts from the Mid-Atlantic Ridge, *J. Volcanol. Geotherm. Res.*

Flower, M. F. J., Robinson, P. T., Ohnmacht, W., and Schmincke, H.-U., 1977. Magma fractionation systems beneath the Mid-Atlantic Ridge, 36-37°N, *Contrib. Mineral. Petrol.*, v. 64, p. 167-195.

Flower, M. F. J., Schmincke, H.-U., Robinson, P. T., Ohnmacht, W., Parker, R., and Gibson, I. L., 1978. Petrology and chemistry of eruptive rocks, DSDP Leg 46. *In* Dmitriev, L., Heirtzler, J., et al., *Initial Reports of the Deep Sea Drilling Project,* v. 46: Washington (U.S. Government Printing Office), p. 425-445.

Hall, J. M., in press. The magnetic properties and magnetization of oceanic basalts and the implications for the history and structure of oceanic Layer 2, *Second Maurice Ewing Symposium, AGU special volume.*

Watkins, N. and Walker, G. F., 1977. Magnetostratigraphy of eastern Iceland, *Am. J. Sci.*, v. 277, p. 513-584.